ImmunoHorizons

RESEARCH ARTICLE | JANUARY 25 2023

Dispensable Role of Aire in CD11c^{+} Conventional Dendritic Cells for Antigen Presentation and Shaping the Transcriptome

Ryuichiro Miyazawa; ... et. al

Immunohorizons (2023) 7 (1): 140–158.
https://doi.org/10.4049/immunohorizons.2200103

ImmunoHorizons

RESEARCH ARTICLE

Adaptive Immunity

Dispensable Role of Aire in CD11c$^+$ Conventional Dendritic Cells for Antigen Presentation and Shaping the Transcriptome

Ryuichiro Miyazawa,* Jun-ichi Nagao,[†,‡] Ken-ichi Arita-Morioka,[†] Minoru Matsumoto,[*,§] Junko Morimoto,* Masaki Yoshida,[¶] Takeshi Oya,[§] Koichi Tsuneyama,[‖] Hideyuki Yoshida,[¶] Yoshihiko Tanaka,[†,‡] and Mitsuru Matsumoto*

*Division of Molecular Immunology, Institute for Enzyme Research, Tokushima University, Tokushima, Japan; [†]Section of Infection Biology, Department of Functional Bioscience, Fukuoka Dental College, Sawara-ku, Fukuoka, Japan; [‡]Oral Medicine Research Center, Fukuoka Dental College, Sawara-ku, Fukuoka, Japan; [§]Department of Molecular Pathology, Tokushima University Graduate School of Biomedical Sciences, Tokushima, Japan; [¶]YCI Laboratory for Immunological Transcriptomics, RIKEN Center for Integrative Medical Science, Yokohama, Japan; and [‖]Department of Pathology and Laboratory Medicine, Tokushima University Graduate School of Biomedical Sciences, Tokushima, Japan

ABSTRACT

Aire, the defect of which is responsible for the development of autoimmunity, is predominantly expressed in medullary thymic epithelial cells, and it controls a wide variety of genes, including those of tissue-restricted Ags, for establishing thymic tolerance. Aire is also expressed from APCs in the periphery, called extrathymic Aire-expressing cells (eTACs), and their complementing role to thymic tolerance has been suggested. eTACs are composed of two distinct classes of APCs, conventional dendritic cell (cDC)–type and group 3 innate lymphoid cell (ILC3)-like–type expressing retinoic acid receptor–related orphan receptor γt (RORγt). Although the essential role of Aire in the latter in the Th17-mediated immune response against *Candida albicans* has been reported, the role of Aire in the cDC-type eTACs for this action has not been examined. Furthermore, the significance of Aire in the production of the transcriptome of the cDC-type eTACs remains unknown. We have approached these issues using a high-fidelity Aire-reporter mouse strain. We found that although the cDC-type eTACs dominated ILC3-like–type eTACs in number and they served as efficient APCs for the immune response against an exogenous Ag as well as for the *C. albicans*–specific Th17 immune response, loss of Aire in cDC-type eTACs showed no clear effect on these functions. Furthermore, loss of Aire showed no major impact on the transcriptome from cDC-type eTACs. These results suggested that Aire in cDC-type eTACs may not have a cell-intrinsic role in the immune response in contrast to the role of Aire in ILC3-like–type eTACs. *ImmunoHorizons*, 2023, 7: 140–158.

Received for publication January 4, 2023. Accepted for publication January 4, 2023.

Address correspondence and reprint requests to: Prof. Mitsuru Matsumoto, Division of Molecular Immunology, Institute for Enzyme Research, Tokushima University, 3-18-15 Kuramoto, Tokushima 770-8503, Japan. E-mail address: mitsuru@tokushima-u.ac.jp

ORCIDs: 0000-0001-5892-7480 (R.M.); 0000-0002-1955-6821 (Minoru Matsumoto); 0000-0002-0670-9868 (K.T.); 0000-0002-6458-5082 (Y.T.); 0000-0003-3844-8110 (Mitsuru Matsumoto).

R.M. and Mitsuru Matsumoto designed the experiments; R.M., J.-I.N., K.-I.A.-K., Minoru Matsumoto, J.M., and Mitsuru Matsumoto conducted the experiments; R.M., Minoru Matsumoto, M.Y., H.Y., and Mitsuru Matsumoto performed RNA-seq and analyzed the data; T.O., K.T., and Y.T. supervised the experiments; and R.M., Minoru Matsumoto, Y.T., and Mitsuru Matsumoto wrote the paper.

The data presented in this article have been submitted to the Gene Expression Omnibus database (https://www.ncbi.nlm.327nih.gov/geo/query/acc.cgi?acc=GSE211006 and https://www.ncbi.nlm.nih.gov/geo/query/acc.cgi?acc=GSE222285) under accession numbers GSE211006 and GSE222285.

This work was supported in part by the Japan Society for the Promotion of Science KAKENHI Grants 19H03699, 22H02892, and 22K19437 (to Mitsuru Matsumoto) and 19K23846 and 20K16287 (to R.M).

Abbreviations used in this article: AGF, human AIRE and GFP-Flag tag; BM, bone marrow; BMDC, bone marrow-derived dendritic cell; cDC, conventional dendritic cell; DC, dendritic cell; EpCAM, epithelial cell adhesion molecule 1; eTAC, extrathymic Aire-expressing cell; FDR, false discovery rate; GO, Gene Ontology; ICOS-L, ICOS ligand; ILC3, group 3 innate lymphoid cell; KI, knockin; KO, knockout; LN, lymph node; LN-DC, DC isolated from LN; MHC-II, MHC class II; MP, membrane protein; mTEC, medullary thymic epithelial cell; RNA-seq, RNA sequencing; RORγt, retinoic acid receptor–related orphan receptor γt; RT, reverse transcription; TMM, trimmed mean of M value; TRA, tissue-restricted Ag; WT, wild-type.

The online version of this article contains supplemental material.

https://doi.org/10.4049/immunohorizons.2200103

ImmunoHorizons is published by The American Association of Immunologists, Inc.

INTRODUCTION

Deficiency for Aire results in the development of organ-specific autoimmune disease associated with chronic mucocutaneous candidiasis, called autoimmune polyendocrinopathy–candidiasis–ectodermal dystrophy (APECED) (OMIM 240300) (1–4). The mechanisms underlying the development of these immunological symptoms, however, have not been fully understood. Aire is predominantly expressed from medullary thymic epithelial cells (mTECs), and transcriptomic analyses using Aire-deficient mTECs demonstrated that Aire controls a wide variety of genes; additionally, much attention has been paid to the genes of tissue-restricted Ags (TRAs) because reduced expression of TRAs in Aire-deficient mTECs could result in the impaired elimination of autoreactive T cells and/or the impaired production of regulatory T cells in an Ag-specific manner (5–8). Besides mTECs, Aire is expressed from APCs in the periphery, named extrathymic Aire-expressing cells (eTACs), and their complementing role to the thymic tolerance mechanisms has been proposed (9). Interestingly, eTACs seem to be a heterogeneous population, and Aire-expressing group 3 innate lymphoid cell (ILC3)–like cells were found besides the conventional dendritic cell (cDC) type of eTACs (10). Indeed, a recent single-cell multiomics approach revealed that there are two major classes of eTACs: a migratory dendritic cell (DC) type of eTACs and eTACs expressing retinoic acid receptor–related orphan receptor γt (RORγt), with the latter corresponding to the Aire-expressing ILC3-like cells (10) and having been named Janus cells (11). The exact identity of Aire-expressing ILC3-like cells, however, is now under debate (12–14) (see *Results*). Recently, the essential role of Aire in the ILC3-like–type eTACs has been demonstrated for the efficient host defense against *Candida albicans* through eliciting the Th17-mediated immune response (15). Furthermore, ILC3-like–type eTACs have been demonstrated to have broad gene expression, including a range of TRAs, with homology to the gene signatures from mTECs (11). Despite the intense characterization of ILC3-like–type eTACs, the role of the cDC type of Aire-expressing cells (cDC-type eTACs) in the protection against *C. albicans* and the production of the transcriptome relevant to the peripheral tolerance remained unknown. Furthermore, phenotypic comparisons between the two types of eTACs using the conventional flow cytometric analysis and immunohistochemical analysis have not been performed.

To gain better insights into the phenotypes of eTACs and to address the role of Aire within them, we have used an Aire-reporter mouse strain in which endogenous Aire was replaced by the human AIRE and GFP-Flag tag (AGF hereafter) fusion protein (Aire/AGF-knockin [KI]) (16). Of note, this Aire-reporter molecule was produced as authentic Aire protein in the form of nuclear dots: this was in marked contrast to the other previously generated Aire-reporter mice in which GFP labeled the whole Aire-expressing cells (i.e., both the cytoplasm and nucleus) (11, 17). Accordingly, Aire/AGF-KI had overcome the molecular gap between the Aire protein (in the nuclei) and reporter molecule (GFP from the whole cells) seen in the conventional Aire-reporter mice by making GFP part of the Aire nuclear dots. This strain faithfully detected not only Aire-expressing mTECs but also eTACs both at a steady state and upon antigenic challenges. More importantly, this strain allows us to distinguish DCs committed to expressing Aire from Aire-nonexpressing DCs in both the presence and absence of functional Aire protein. This was because the AGF reporter molecule showed no function of Aire according to their disease phenotypes (16): mice harboring a combination of the Aire-null allele and AGF allele (i.e., −/AGF allele) on a NOD background showed a typical autoimmune attack against pancreatic acinar cells, a characteristic of Aire-deficient mice on a NOD background (18, 19). In contrast, heterozygous Aire/AGF-KI (+/KI) did not show any Aire-deficient phenotypes, indicating that the AGF reporter molecule had no dominant-negative effect on the wild-type (WT) allele. This allowed us to use heterozygous Aire/AGF-KI (+/KI) as Aire-sufficient mice. With this high-fidelity Aire-reporter strain, we have characterized two types of eTACs, that is, cDC-type and ILC3-like–type eTACs. In the current study, we particularly focused on the cell-intrinsic role of Aire in the cDC-type of eTACs in induction of the Th17 immune response against *C. albicans* and the production of transcriptome from them. Our studies have illuminated the distinct role of Aire in cDC-type eTACs and ILC3-like–type eTACs by demonstrating the dispensable role of Aire in the cDC-type eTACS.

MATERIALS AND METHODS

Mice

Aire/AGF-KI mice (16) and Aire-knockout (KO) mice (20), both on C57BL/6 backgrounds, were generated by homologous recombination in embryonic stem cells as previously described. Mice were maintained under pathogen-free conditions and treated in accordance with the Guidelines for Animal Experimentation of Tokushima University School of Medicine.

Preparation of lymph node cell suspension and flow cytometric analysis

The inguinal, axillary, and cervical lymph nodes (LNs) were digested with collagenase D (Roche)/DNase I (Roche) in RPMI 1640 medium containing 10% FBS, 1% nonessential amino acids solution (Life Technologies), 1% sodium pyruvate (Life Technologies), 20 mM HEPES (Life Technologies), 0.1 mg/ml penicillin-streptomycin mixed solution (Nacalai Tesque) and 50 μM 2-ME (Sigma-Aldrich), hereafter referred to as R10, at room temperature for 30 min. The suspension was homogenized by pipetting up and down to release the cells including the DCs. Then, LN cells were suspended in PBS containing 1% BSA and 5 mM EDTA and incubated with anti-CD16/32 (clone 96) mAb for Fc blocking followed by staining with mAbs against CD45 (clone 30-F11), CD11c (clone N418), CD11b (clone

https://doi.org/10.4049/immunohorizons.2200103

M1/70), CD8 (clone 53-6.7), and I-A/I-E (clone M5/114.15.2). mAbs against CD16/32, CD45, CD11c, CD11b, and CD8 were purchased from BioLegend. A mAb against I-A/I-E was purchased from eBioscience.

Generation of bone marrow–derived DCs and flow cytometric analysis

Bone marrow (BM) cells were prepared as previously described (21). In brief, BM cells from femurs of mice were harvested with R10 and RBCs were lysed in RBC lysis buffer by hypotonic shock. BM cells adjusted to 1×10^6 cells/ml in the R10 were supplemented with 20 ng/ml recombinant murine GM-CSF (Miltenyi Biotec) and 10 ng/ml recombinant murine IL-4 (PeproTech). Then, 2×10^6 BM cells per well in 12-well plates (Thermo Fisher Scientific) were cultured at 37°C in a 5% CO_2 environment for 60 h. Then, bone marrow-derived dendritic cells (BMDCs) were stained with the following mAbs for flow cytometric analysis. Cells were incubated with anti-CD16/32 (clone 96) mAb for Fc blocking followed by staining with B220 (clone RA3-6B2) and mAbs against CD11c (clone N418), CD11b (clone M1/70), CD24 (clone M1/69), and I-A/I-E (clone M5/114.15.2). B220 and anti-CD24 mAbs were purchased from BioLegend.

Flow cytometric analysis and FACS sorting

Flow cytometric analysis was performed using a FACSAria II (BD Biosciences) as described previously (17). For the staining of cell surface molecules, mAbs against CD80 (clone 16-10A1), CD86 (clone GL1), ICOS ligand (ICOS-L; clone HK5.3), CD40 (clone 3/23), CD127 (clone A7R34), PD-L1 (clone B7-H1), CCR7 (clone 4B12), CD200 (clone OX2), epithelial cell adhesion molecule 1 (EpCAM; clone G8.8), CD14 (clone Sa14-2), CD64 (clone X54-5/7.1), and Gr-1 (clone RB6-8C5) purchased from BioLegend were used. For intercellular staining, mAb against RORγt (clone Q31-378) purchased from BD Biosciences was used after fixation and permeabilization with an eBioscience Foxp3/transcription factor staining buffer set (eBioscience). AGF^+ and AGF^- DCs isolated from LNs (LN-DCs) gated for $CD45^+CD11c^+$MHC class II $(MHC\text{-}II)^+$ fraction were sorted by a FACSAria II. AGF^+ BMDCs gated for the $B220^-CD24^+CD11b^{-/low}$ fraction and AGF^- BMDCs gated for the $B220^-CD11c^+MHC\text{-}II^+$ fraction were sorted by a FACSAria II. Sorted cells were examined with immunocytochemical analysis, a T cell proliferation assay, and RNA sequencing (RNA-seq). Data were analyzed using FlowJo 10.8.1 software (Tree Star).

Immunocytochemical analysis

Immunohistochemical staining was performed as described previously (22). The inguinal LNs from Aire/AGF-KI were harvested and embedded in OCT compound (Sakura Finetek) and frozen at −80°C. Cryosections (6 μm) prepared from frozen tissue were fixed with acetone. The samples were blocked with 1% BSA containing PBS at room temperature for 30 min followed by staining with anti-GFP polyclonal Ab, anti-CD11c (clone N418) mAb, and anti-RORγt (clone B2D) mAb at room temperature for 90 min. The samples were then washed with PBS five times and nuclei were stained with DAPI (Sigma-Aldrich). The samples were mounted with ProLong Gold mounting medium (Life Technologies). The polyclonal Ab against GFP and mAbs against CD11c and RORγt were purchased from Invitrogen, BioLegend, and eBioscience, respectively. The sections were examined for fluorescence microscopy analysis using a BZ-X810 all-in-one fluorescence microscope and BZ-X810 analyzer software (Keyence, Osaka, Japan).

Cytology and cell staining

FACS-sorted LN-DCs and BMDCs were attached to the glass slides and fixed with acetone after the cells dried. Then, the samples were blocked with 1% BSA containing PBS at room temperature for 30 min followed by staining with anti-GFP polyclonal Ab and anti-Aire mAb (clone 5H12) (Invitrogen). The samples were then washed with PBS five times and nuclei were stained with DAPI (Sigma-Aldrich). Samples were mounted with mounting medium.

Ag-presenting capacity and T cell proliferation

CFSE labeling and a T cell proliferation assay were performed as described previously (23). Splenic $CD4^+$ T cells from OT-II mice (OVA-specific TCR transgenic mice) (24) were collected with magnetic cell sorting (Miltenyi Biotec) followed by labeling with CFSE. Then, CSFE-labeled OT-II $CD4^+$ T cells were cultured with FACS-sorted DCs at a 10:1 ratio in the presence of OVA protein for 72 h. CFSE dilutions in OT-II $CD4^+$ T cells were assayed by a FACSAria II (BD Biosciences).

In vivo priming with C. albicans *mycelial membrane protein fraction and in vitro* $CD4^+$ *T cell differentiation*

A 100 μg/ml *C. albicans* mycelial membrane protein (MP) fraction from *C. albicans* SC5314 (25) was prepared as previously described (26). Then, 200 μl of a 1:1 emulsion of *C. albicans* mycelial MP fraction and CFA (*Candida*/CFA) was injected into mice (s.c.). Alternatively, a 1:1 emulsion of PBS and CFA (PBS/CFA) was injected into the control mice. Mice immunized with *Candida*/CFA or PBS/CFA were sacrificed on day 6. $CD4^+$ T cells from LN and spleen were collected with MACS CD4 MicroBeads (Miltenyi Biotec) according to the manufacturer's instructions. $AGF^{+/-}$ DCs and $CD4^+$ T cells from *Candida*/CFA-injected mice were cultured with a 1:2 ratio in the presence or absence of a 2.5 μg/ml *C. albicans* mycelial MP fraction for 6 d. Then, samples were collected and restimulated with 500 ng/ml ionomycin (Sigma-Aldrich) and 50 ng/ml PMA (Sigma-Aldrich) in the presence of 10 μg/ml brefeldin A (Sigma-Aldrich) and inhibiting the cytokine secretion for 4 h at 37°C. Cells were suspended in PBS containing 1% BSA and 5 mM EDTA and incubated with anti-CD16/32 (clone 96) mAb for Fc blocking followed by staining with anti-CD4 mAb (GK1.5). Then, the cells were fixed and permeabilized with an

eBioscience Foxp3/transcription factor staining buffer set. Intracellular cytokines were stained with anti–IFN-γ (XMG1.2) and anti–IL-17A (TC11-18H10.1). Flow cytometric analysis was performed using a FACSAria II (BD Biosciences).

In vivo priming with live C. albicans *and in vitro CD4*$^+$ *T cell differentiation*

C. albicans SC5314 was cultured on a YPD agar plate (1% yeast extract, 2% Bacto peptone, 2% glucose, and 1.5% agar) for 48 h at 37°C as previously described (26). We performed an intragastric injection of *C. albicans* (2×10^8 cells/mice) for in vivo priming. For control mice, PBS was injected. Ten days after intragastric injection of *C. albicans*, CD4$^+$ T cells from LN and spleen were collected with MACS CD4 MicroBeads (Miltenyi Biotec) according to the manufacturer's instructions. AGF$^{+/-}$ BMDCs and CD4$^+$ T cells from *C. albicans* intragastrically injected mice were cocultured with a 1:2 ratio in the presence or absence of 1.25×10^6 cells/ml of heat-killed *C. albicans* for 6 d in 96-well plates. Restimulation of CD4$^+$ T cells and flow cytometric analysis were performed as described above.

Real-time PCR

Total RNA was extracted from FACS-sorted CD11c$^+$AGF$^+$ LN-DCs and CD11c$^-$AGF$^+$ LN-DCs on CD45$^+$lineage$^-$ (CD3, CD19, B220, and Gr-1) with ReliaPrep RNA miniprep systems (Promega) and converted to cDNA with a high-capacity cDNA reverse transcription (RT) kit (Thermo Fisher Scientific) according to the manufacturer's protocols and guidelines. mRNA expression analysis was performed using a QuantiTect probe PCR kit (Qiagen) on a Thermal Cycler Dice real-time system II (Takara Bio). The following primers and dual-labeled probes (FAM/TAMRA) were used: *Aire* primers, forward, 5′-GGAGGATTCTCTTTAAGGACTACAA-3′, reverse, 5′-CTGGTTTAGGTCCACATCTTTTGG-3′, probe, 5′-TACAGCCGCCTGCATAGCATCCTGGA-3′; *Rorc* primers, forward, 5′-CTGCCCCATTGACCGAACC-3′, reverse, 5′-GCCAAACTTGACAGCATCTCG-3′, probe, 5′-AACCGATGCCAGCATTGCCGCCT-3′; *Hprt* primers, forward, 5′-TGAAGAGCTACTGTAATGATCAGTCAAC-3′, reverse, 5′-AGCAAGCTTGCAACCTTAACCA-3′, probe, 5′-GGGTTAAGCAGTACAGCCCCA-3′.

RNA preparation and RNA-seq

RNA-seq libraries were prepared by applying a random displacement amplification sequencing method for single-cell RNA-seq (27). Specifically, AGF$^+$ and AGF$^-$ DCs from LNs were sorted for the CD45$^+$CD11c$^+$MHC-II$^+$ fraction by FACSAria II. AGF$^+$ BMDCs in a B220$^-$CD24$^+$CD11b$^{-/low}$ fraction and AGF$^-$ BMDCs in a B220$^-$CD11c$^+$MHC-II$^+$ fraction were also sorted into a tube containing lysis buffer (buffer TCL, Qiagen). Total RNAs from the cells were isolated using RNAClean XP beads (Beckman Coulter) directly from the lysis buffer and were eluted into 10 μl of water containing RNase inhibitor (4 U/μl RNasin Plus RNase inhibitor, Promega). The RNA was denatured by incubating at 65°C for 5 min, then placement on ice and treatment with DNase I (0.1 U/μl DNase I, amplification grade, Invitrogen) in 0.25× RT buffer (PrimeScript RT reagent kit, Takara Bio) at 30°C for 15 min. Then, cDNA was synthesized in 30 μl of 1× RT buffer containing RT enzyme mix (1.5 μl of PrimeScript RT enzyme mix I, Takara Bio), oligo(dT)-RT primer (0.2 μM Oligo(dT)18 primer, Thermo Scientific), T4 gene 32 protein (0.033 mg/ml, NEB), and first NSR (not-so-random) primer mix for mice (3.3 μM, Sigma-Aldrich custom DNA oligonucleotides) by incubating for 10 min at 25°C, 10 min at 30°C, 30 min at 37°C, 5 min at 50°C, and 5 min at 94°C. Next, the second strand was synthesized by adding 5 μl of 10× NEB buffer 2 (NEB), 1.25 μl of 2′-deoxynucleoside 5′-triphosphate mix (10 mM each nucleotide, NEB), 1.5 μl of Klenow fragment (3′→5′ exo$^-$, NEB), 5 μl of second NSR primer for mice (100 μM, Sigma-Aldrich custom DNA oligonucleotides), and 7.25 μl of distilled water and incubating for 60 min at 16°C followed by 10 min at 70°C. The ds-cDNA was purified using the AMPure XP beads (Beckman Coulter) and quantified using Qubit (Qubit dsDNA HS assay kit, Invitrogen). Then, ds-cDNA <1 ng was applied for Tn5 tagmentation in a 25-μl reaction with a homemade Tn5 enzyme prepared as previously described (28, 29). DNA was purified using AMPure XP beads and amplified by 10–15 cycles of PCR using indexed primers and KAPA HiFi DNA polymerase (Roche). The libraries were purified using AMPure XP beads and pooled for next-generation sequencing on an Illumina HiSeq system.

Method for informatics

After trimming low-quality reads and adapter sequences by fastp (30), short reads were mapped to mm10 by star (version 2.7.3a) (31) employing an Ensembl GTF file for mm10 downloaded from https://www.ensembl.org. Unmapped reads and reads mapped with a low-quality score (mapping quality <5) were removed using samtools (version 1.9) (32), and duplicated reads were removed by Picard MarkDuplicates (http://broadinstitute.github.io/picard). Mapped reads on each transcript were counted using htseq-count (version 0.11.2) (33) with -stranded = no option and an Ensembl GTF file for mm10. Raw read counts on transcripts were processed using R with the edgeR package (version 3.20.9) (34) for normalization and to identify differentially expressed genes. The FASTQ data of mTEC^{high} were extracted from the Gene Expression Omnibus database under accession number GSE222285 and processed by the same analytic pipeline as DC samples. TRAs were defined as genes expressed in less than three tissues. Heatmaps were visualized using R with the ComplexHeatmap package (version 2.12.0) (35). Gene Ontology (GO) analysis and gene set enrichment analysis of a gene set was performed using R with the clusterProfiler package (version 3.6.0) (36). The dataset associated with this project has been submitted to the Gene Expression Omnibus database (https://www.ncbi.nlm.nih.gov/geo/query/acc.cgi?acc=GSE211006 and https://www.ncbi.nlm.nih.gov/geo/query/acc.cgi?acc=GSE222285).

Statistical analysis

Statistical comparisons within two groups were examined with a two-tailed Student *t* test. One-way ANOVA was used for more than three groups. A p value <0.05 was considered statistically significant.

RESULTS

Two distinct types of Aire-expressing APCs in the LNs

To characterize the Aire-expressing cells in the periphery, eTACs, we used heterozygous Aire/AGF-KI (16). Enzymatic digestion of LNs showed the GFP signals from two distinct populations after gating for $CD3^-CD19^-B220^-Gr\text{-}1^-$ cells: major $CD45^+AGF^+$ hematopoietic cells and minor $CD45^-AGF^+$ stromal cells (Fig. 1A, lower left). When $CD45^+AGF^+$ cells were evaluated for CD11c expression, we observed a $CD11c^{high}$ population (Fig. 1A, lower middle, squared in red) and a $CD11c^{-/low}$ population (Fig. 1A, lower middle, squared in black). The signal intensity of GFP from the former was weaker compared with the latter. When the same $CD45^+AGF^+$ cells were evaluated for RORγt expression, we observed a major $ROR\gamma t^{low\ to\ int}$ population (Fig. 1A, lower right, squared in red) and a minor $ROR\gamma t^{high}$ population (Fig. 1A, lower right, squared in black): the signal intensity of GFP from the former was weaker than the latter. When the $CD45^+AGF^+$ cells were evaluated for their simultaneous expression of CD11c and RORγt, three major populations emerged: $CD11c^+ROR\gamma t^-$, $CD11c^-ROR\gamma t^+$, and $CD11c^-ROR\gamma t^-$ cells (Fig. 1B, middle). In contrast, $CD45^-AGF^+$ cells were mostly $CD11c^-ROR\gamma t^-$ (Fig. 1B, right). We focused on the $CD45^+$ hematopoietic cells in this study.

$CD11c^+ROR\gamma t^-$ cells (~60%) dominated $CD11c^-ROR\gamma t^+$ cells (~10%) among the $CD45^+AGF^+$ cells in numbers (Fig. 1C), the ratio of which was within the range of the previous report: the ratio between the $Aire^+Rorc^-$ cells and $Aire^{high}Rorc^+$ cells revealed by the single-cell multiomics was ~8:1 (11). The authors originally reported that both $Aire^+Rorc^-$ and $Aire^{high}Rorc^+$ cells had high transcriptional similarity to migratory DCs (11). However, their exact identity, especially for the latter, is now under debate because $ROR\gamma t^+$ APCs have been reported to play an important role in the generation of commensal-specific peripheral regulatory T cells (12–14). Based on these circumstances, we tentatively named Aire-expressing $CD11c^+ROR\gamma t^-$ cells and Aire-expressing $CD11c^-ROR\gamma t^+$ cells in the LNs $CD11c^+$ Aire-DCs and $ROR\gamma t^+$ Aire-APCs, respectively. Real-time PCR analyses demonstrated that the expression level of *Aire* was ~3-fold higher in $ROR\gamma t^+$ Aire-APCs compared with $CD11c^+$ Aire-DCs (Fig. 1D, left), consistent with the stronger GFP signals from $ROR\gamma t^+$ Aire-APCs compared with those from the $CD11c^+$ Aire-DCs (Fig. 1A). The expression level of *Rorc* was much higher in $ROR\gamma t^+$ Aire-APCs compared with $CD11c^+$ Aire-DCs, as expected (Fig. 1D, right).

Both $CD11c^+$ Aire-DCs and $ROR\gamma t^+$ Aire-APCs expressed AGF nuclear dots that showed the colocalization with endogenous Aire by immunocytochemical analysis (Fig. 1E), although the numbers of AGF nuclear dots were much fewer compared with those from mTECs (R. Miyazawa and Mitsuru Matsumoto, unpublished observation). Furthermore, we did not detect clear AGF dots in many $CD11c^+$ Aire-DCs and in $ROR\gamma t^+$ Aire-APCs probably due to the relatively weak Aire expression. Morphologically, we did not notice any clear difference between $CD11c^+$ Aire-DCs and $CD11c^-$ Aire-APCs (i.e., $ROR\gamma t^+$ Aire-APCs) when stained with May–Giemsa, both showing a rather narrow cytoplasm typical for cDCs (Fig. 1E, *rightmost*). We also evaluated the location of Aire-expressing APCs within the LNs (LN-DCs or LN-APCs in short hereafter) by immunohistochemistry. $CD11c^+$ Aire-DCs were located predominantly within the T cell areas whereas $ROR\gamma t^+$ Aire-APCs existed mainly in the interfollicular spaces (Fig. 1F). Similar to the $CD11c^+$ Aire-DCs in the LNs, Aire-expressing marginal zone DCs in the spleen were reported outside the B cell follicles (37). Although $CD11c^+$ Aire-DCs dominated $ROR\gamma t^+$ Aire-APCs in number (Fig. 1C), $ROR\gamma t^+$ Aire-APCs in the interfollicular spaces looked more prominent compared with $CD11c^+$ Aire-DCs in the T cell areas due to the stronger GFP signals (Fig. 1F). The location of $CD11c^+$ Aire-DCs and $ROR\gamma t^+$ Aire-APCs in LNs was not different between heterozygous (+/KI) and homozygous Aire/AGF-KI (KI/KI, in which functional Aire protein is absent) (16). The results suggested that Aire in APCs does not have a major impact on their location in a cell-autonomous fashion (Supplemental Fig. 1A).

Characterization of $CD11c^+$ Aire-DCs

Because $CD11c^+$ Aire-DCs formed a major population of Aire-expressing cells in the LNs and $ROR\gamma t^+$ Aire-APCs were characterized in the other studies (10, 12–15), we focused on the characterization of $CD11c^+$ Aire-DCs. LN suspensions gated for the $CD45^+CD11c^+MHC\text{-}II^{high}$ fraction contained the $Aire^+$ DCs (corresponding to the $CD11c^+$ Aire-DCs but not to $ROR\gamma t^+$ Aire-APCs because of the $CD11c^+$ gating strategy) (Fig. 2A, left). They expressed Sirpα at the intermediate level (Fig. 2A, *right*). To test which type of DCs (i.e., $CD8^+CD11b^-$ [cDC1s] or $CD8^-CD11b^+$ [cDC2s]) (38) express Aire, we divided the $CD45^+CD11c^+MHC\text{-}II^{high}$ fraction into $Aire^+$ (AGF^+) and $Aire^-$ (AGF^-) DCs (Fig. 2B). Although both $Aire^+$ and $Aire^-$ DCs had more $CD8^-CD11b^+$ type than $CD8^+CD11b^-$ type, it was less evident in the $Aire^+$ DCs (the ratio of $CD8^+CD11b^-$ versus $CD8^-CD11b^+$ was ~1:3) compared with $Aire^-$ DCs (which was an ~1:7 ratio) (Fig. 2B). Thus, $CD11c^+$ Aire-DCs were composed of both cDC1s and cDC2s and they were slightly skewed toward cDC1s when compared with Aire-nonexpressing DCs.

Because Aire deficiency confers high susceptibility to *C. albicans* infection of the mouth and esophagus, we compared the numbers of $CD11c^+$ Aire-DCs in the cervical LNs with those in the LNs from other portions (i.e., inguinal and axillary LNs). We found that cervical LNs contained significantly higher percentages of $CD11c^+$ Aire-DCs compared with LNs from the other portions (Fig. 2C, left). Higher frequencies of $CD11c^+$ Aire-

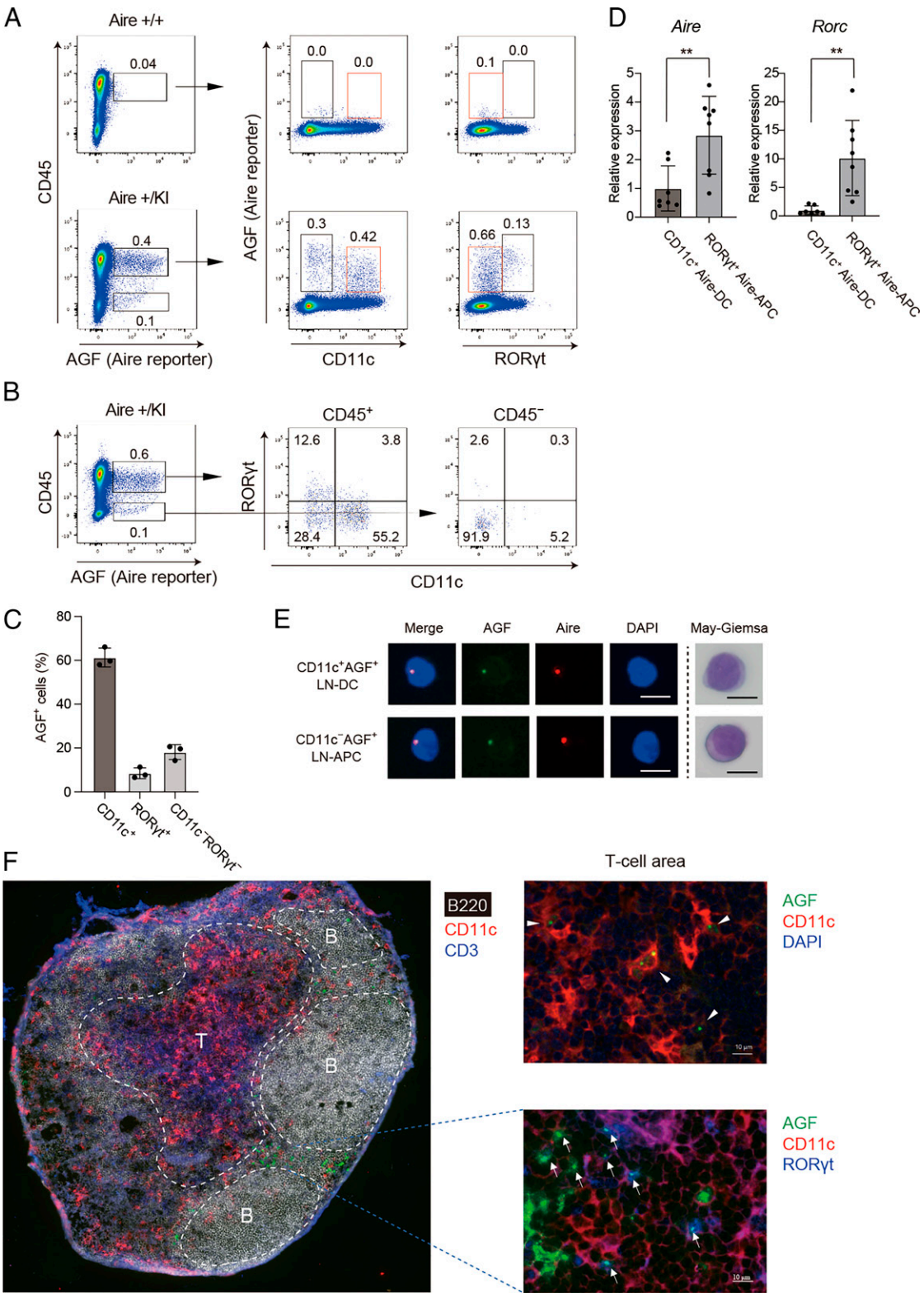

FIGURE 1. Two distinct types of Aire-expressing APCs in the LNs.

(**A**) LN cell suspensions prepared from Aire$^{+/+}$ and Aire$^{+/KI}$ were gated for lineage^{-} (CD3, CD19, B220, and Gr-1) cells and were evaluated for the expression of AGF, CD45, CD11c, and RORγt. CD11c^{+} Aire-DCs and RORγt^{+} Aire-APCs were squared in red and black, respectively (lower middle and lower right). One representative result from more than three repeats is shown. (**B**) LN cell suspensions prepared from Aire$^{+/KI}$ in (A) were simultaneously evaluated for their expression of CD11c and RORγt after dividing into CD45^{+} and CD45^{-} cells. One representative result ***(Continued)***

https://doi.org/10.4049/immunohorizons.2200103

DCs in the cervical LNs than in other peripheral LNs remained constant over age, which was also observed in the absence of Aire (KI/KI) (Supplemental Fig. 1B). Cervical LNs contained a lower proportion of $CD8^+CD11b^-$ cDC1 type of $CD11c^+$ Aire-DCs compared with other peripheral LNs (Fig. 2C, right).

Besides cDC1/cDC2 classification, DCs in the LNs can be divided into migratory DCs and resident DCs depending on their expression of the chemokine receptor CCR7 (39, 40). When LN-DCs from WT mice were stained with mAbs against MHC-II and CD11c, $CCR7^{high}$ migratory DCs showed slightly higher expression of MHC-II with lower expression of CD11c compared with $CCR7^{low}$ resident DCs (Fig. 2D). Conversely, $CCR7^{low}$ resident DCs showed a slightly lower expression of MHC-II with higher expression of CD11c compared with $CCR7^{high}$ migratory DCs. We examined to which type $CD11c^+$ Aire-DCs correspond. We found that almost half of the $CD11c^+$ Aire-DCs (gated for $CD45^+CD11c^+$MHC-II^{high}) showed $CCR7^{high}$ expression (migratory type) and the remainder showed $CCR7^{low}$ expression (resident type) (Fig. 2E, left), indicating that $CD11c^+$ Aire-DCs did not solely belong to either type. Instead, $CD11c^+$ Aire-DCs contained both migratory and resident types. Thus, all of the non-ILC3-like–type eTACs did not show a migratory phenotype in contrast to the nomenclature proposed based on the single-cell multiomics analysis (11). AGF^- DCs also contained both migratory and resident types at a similar ratio (Fig. 2E, right).

We then examined the expression of surface molecules including those important for Ag presentation. The expression level of CD86 was slightly higher in $CD11c^+$ Aire-DCs (in red) compared with those from $Aire^-$ DCs (in blue) (the same gating strategy for $Aire^-$ DCs was used as in collecting the $CD11c^+$ Aire-DCs except for AGF expression) (Fig. 2F, upper). Although less evident, the expression levels of CD40 and ICOS-L were also higher in $CD11c^+$ Aire-DCs than in $Aire^-$ DCs. Because the initial study reported several molecules unique to eTACs in humans (41), we also evaluated the expression of these surface molecules. Consistent with the previous reports in both humans (41) and mice (11), we observed higher expression of CD127, PD-L1, and CD200 from $CD11c^+$ Aire-DCs compared with $Aire^-$ DCs (Fig. 2F, lower). Interestingly, the expression levels of EpCAM were higher in $CD11c^+$ Aire-DCs than in the $Aire^-$ DCs, which could be one possible reason for the initial confusion about the eTACs as a stromal origin (9).

In vitro induction of Aire-expressing DCs from the BM

Knowing that DCs are the major component of eTACs, we tried to induce the BMDCs that express Aire using Aire/AGF-KI. We cultured BM cells isolated from the heterozygous Aire/AGF-KI supplemented with several cytokines to produce the AGF^+ BMDCs. Among the several cytokines tested, we could induce AGF^+CD103^- BMDCs most efficiently using the combination of GM-CSF plus IL-4 and/or GM-CSF plus IL-4 plus Flt3L (Supplemental Fig. 1C, upper). AGF signals from the BM cells appeared as early as 2 d after the culture, and it was almost the peak of the AGF expression: ∼5–8% of the cells expressed AGF on day 2, and AGF signals gradually declined on day 4 (∼2.5%) followed by day 6 (∼2.0%). Because the addition of Flt3L did not improve the efficiency of producing AGF^+ BMDCs significantly, subsequent experiments were performed without Flt3L, that is, a combination of GM-CSF and IL-4 (Supplemental Fig. 1C).

We characterized $Aire^+$ BM-DCs more in detail. Because cultured BMDCs can be classified into three major populations depending on their expression of CD11b and CD24 ($CD11b^-CD24^{med/+}$, $CD11b^+CD24^+$, and $CD11b^+CD24^{low/-}$) (42), we first examined which fraction contained the $Aire^+$ BMDCs (Fig. 3A). $Aire^+$ BMDCs were present almost exclusively in the $CD11b^-CD24^{med/+}$ fraction. $Aire^+$ BMDCs scarcely expressed CD11c, and their RORγt expression level was low to intermediate (i.e., $CD11c^{-/low}$RORγt$^{low\ to\ int}$) (Fig. 3B). This phenotype of $Aire^+$ BMDCs does not represent simply either $CD11c^+$ Aire-DCs or $ROR\gamma t^+$ Aire-APCs from LNs. Rather, $Aire^+$ BM-DCs showed a hybrid of the characteristics representing the two types of $Aire^+$ APCs in that they expressed neither CD11c nor RORγt at high levels (see Fig. 1A). Importantly, however, note that $Aire^+$ BMDCs are myeloid but not ILCs in light of the fact that they were expanded upon GM-CSF stimulation.

We then evaluated the expression of molecules involved in the Ag presentation from $Aire^+$ BMDCs that appeared in the $B220^-CD11b^-CD24^{med/+}$ fraction from heterozygous Aire/AGF-KI (+/KI). $Aire^+$ BMDCs homogenously expressed MHC-II at high levels (Fig. 3C, top in red). In contrast, $Aire^-$ BM-DCs in

from more than three repeats is shown. (**C**) The composition of two distinct types of $Aire^+$ DCs analyzed in (B). Data were plotted from three independent experiments. Bars indicate means ± SD. (**D**) Real-time PCR analyses of *Aire* and *Rorc* from FACS-sorted $CD11c^+AGF^+$ DCs ($CD11c^+$ Aire-DCs) and $CD11c^-AGF^+$ APCs ($ROR\gamma t^+$ Aire-APCs) after gating for $CD45^+$lineage$^-$ cells isolated from the LNs in $Aire^{+/KI}$. The expression level of *Hprt* was used as an internal control for RNAs. Data were collected from more than three independent experiments. Bars indicate means ± SD. $^{**}p < 0.01$. (**E**) Expression of Aire protein from FACS-sorted AGF^+CD11c^+ DCs and AGF^+CD11c^- APCs isolated from LNs (LN-DCs and LN-APCs). Cells were stained with anti-GFP and anti-Aire Abs. Nuclei were stained with DAPI. May–Giemsa solution was used for the counterstaining. Scale bars, 10 μm. One representative result from more than three repeats is shown. (**F**) Identification of $Aire^+$ DCs in LNs by immunohistochemical analysis. Sections of inguinal LN were stained with B220 (white), anti-CD11c (red), and anti-CD3 (blue) mAbs (left). Higher magnification of AGF^+ cells in the T cell area, representing $CD11c^+$ Aire-DCs (upper), and interfollicular spaces, representing $ROR\gamma t^+$ Aire-DCs (lower), are shown on the right. Nuclei were stained with DAPI in blue, and arrowheads indicate AGF^+CD11c^+ DCs (upper right). Arrows indicate $AGF^+CD11c^{-/low}ROR\gamma t^+$ DCs (lower right). One representative result from more than three repeats is shown. Scale bars, 10 μm.

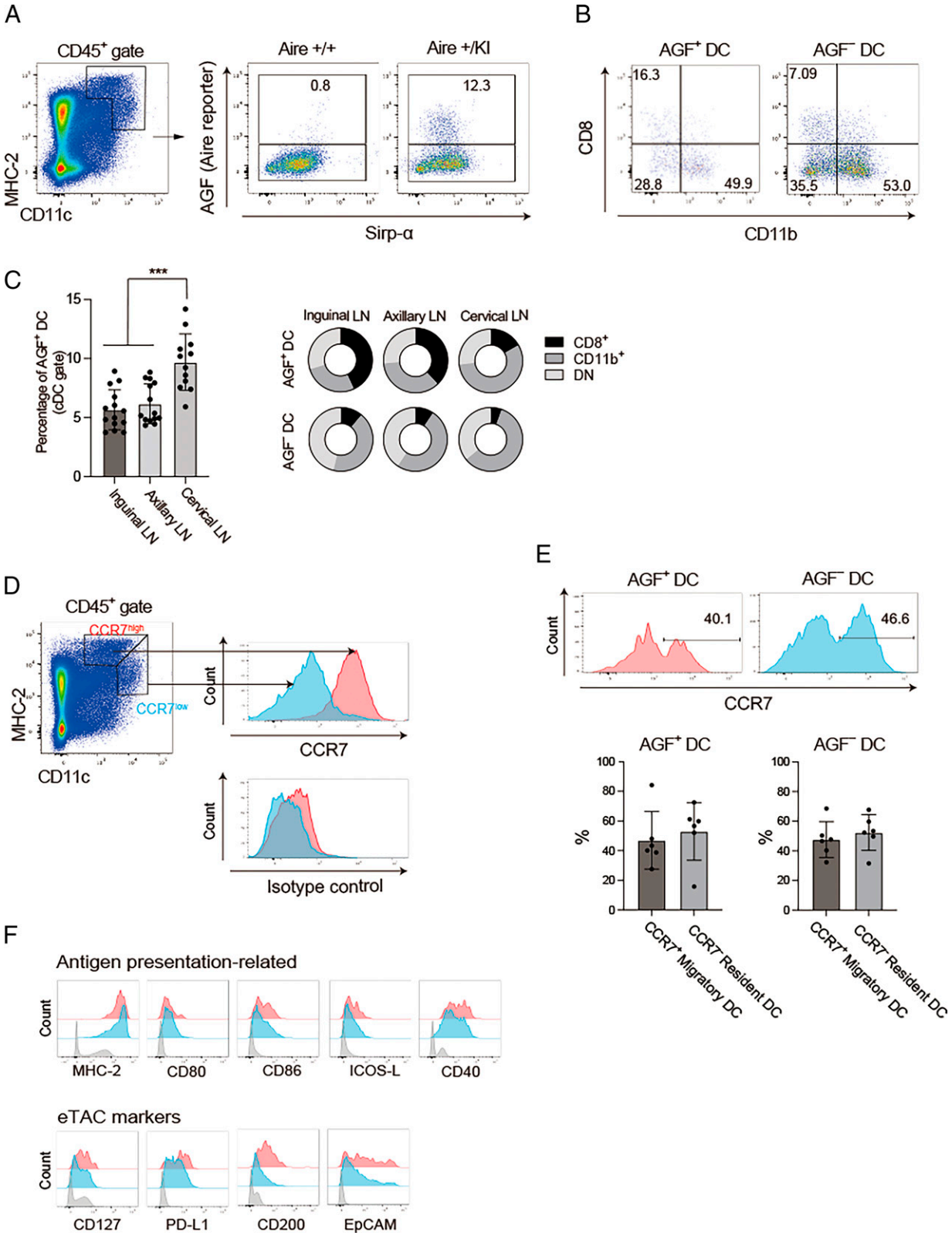

FIGURE 2. Characterization of CD11c$^+$ cDCs expressing Aire.

(**A**) Expression of Sirpα from CD11c$^+$ Aire-DCs in cervical LNs. Cells were gated for the CD45$^+$CD11c$^+$MHC-II^{high} fraction. One representative result from more than three repeats is shown. (**B**) Both CD11c$^+$ Aire-DCs and Aire-nonexpressing DCs (AGF$^-$ DCs) had more CD8$^-$CD11b$^+$ type (cDC2s) than CD8$^+$CD11b$^-$ type (cDC1s), although CD11c$^+$ Aire-DCs were slightly skewed toward the cDC1 type compared with AGF$^-$ DCs. ***(Continued)***

https://doi.org/10.4049/immunohorizons.2200103

the same fraction expressed MHC-II at variable levels ranging from negative to high, although MHC-II$^-$ cells dominated the MHC-II$^+$ cells (Fig. 3C, top in blue). Expression levels of CD80, CD86, ICOS-L, and CD40 were also higher in Aire$^+$ BM-DCs compared with Aire$^-$ BM-DCs. Of note, the expression levels of these molecules (i.e., CD80, CD86, ICOS-L, and CD40) were more evident even when compared with those from the primary Aire$^+$ DCs in LNs (compare Fig. 3C, top with Fig. 2F, upper). Expression of CD127, CCR7, and CD200 was also higher in Aire$^+$ BMDCs compared with Aire$^-$ counterparts, although the expression levels of PD-L1 and EpCAM were indistinguishable between Aire$^+$ and Aire$^-$ BM DCs (Fig. 3C, middle). Expression of the markers for monocytes/macrophages (CD14, CD64, and Gr-1) was negative for the Aire$^+$ BMDCs (Fig. 3C, bottom). Aire$^+$ BMDCs expressed a single dot of AGF protein in most cases that were colocalized with endogenous Aire (Fig. 3D), although we did not detect clear AGF dots in many Aire$^+$ BMDCs (R. Miyazawa and Mitsuru Matsumoto, unpublished observation). Morphologically, Aire$^+$ BMDCs showed broader cytoplasm exhibiting a brighter Giemsa staining compared with Aire$^-$ BMDCs (Fig. 3D, rightmost).

Although Aire$^+$ BMDCs expressed higher levels of the molecules for Ag presentation compared with their Aire$^-$ counterpart that appeared in the CD11b$^-$CD24$^{med/+}$ fraction (Fig. 3A), we found that Aire expression was not a prerequisite for the expression of the molecules related to the Ag presentation. When the expression of these molecules (MHC-II, CD80, CD86, ICOS-L, and CD40) was assessed from the cultured AGF$^+$ BMDCs established from homozygous Aire/AGF-KI (in which there is no functional Aire protein) (Fig. 3E, upper in blue), it was comparable to those from Aire-sufficient heterozygous Aire/AGF-KI (Fig. 3E, upper in red). Thus, Aire may not be required for promoting the ability of Ag presentation (see below). In contrast, expression of CD127 and CD200 was slightly higher in Aire-sufficient AGF$^+$ BMDCs from heterozygous Aire/AGF-KI compared with that from Aire-deficient AGF$^+$ BMDCs from homozygous Aire/AGF-KI (Fig. 3E, lower). Thus, expression of CD127 and CD200 might be a unique feature of Aire-expressing DCs as we have seen in LN-DCs (Fig. 2F, lower).

The Ag-presenting capacity of CD11c$^+$ Aire-DCs and Aire$^+$ BMDCs

We then examined the Ag-presenting capacity of Aire$^+$ DCs, that is, CD11c$^+$ Aire-DCs and Aire$^+$ BMDCs, using the TCR-transgenic system (24). For CD11c$^+$ Aire-DCs, we mixed CFSE-labeled transgenic CD4$^+$OT-II T cells specific for OVA peptide with AGF$^+$CD11c$^+$MHC-II^{high} cells isolated from the LNs (corresponding to the CD11c$^+$ Aire-DCs) at a 10:1 ratio. When OVA protein was added into the culture (10 μg/ml), we observed the proliferation of OT-II T cells (Fig. 4A, uppermost), indicating that CD11c$^+$ Aire-DCs have the capacity for Ag processing and presentation. Importantly, however, note that AGF$^-$CD11c$^+$MHC-II^{high} cells (the same gating strategy was used as in collecting the CD11c$^+$ Aire-DCs except for AGF expression) also induced the proliferation of OT-II T cells in the presence of OVA to a similar degree (Fig. 4A, third upper). More importantly, when AGF$^+$CD11c$^+$MHC-II^{high} cells (corresponding to the CD11c$^+$ Aire-DCs on the Aire-sufficient background) were isolated from the Aire-deficient background (−/KI) (called Aire$^{less\text{-}AGF}$ cells hereafter), they could also induce the proliferation of OT-II T cells in the presence of OVA protein (Fig. 4A, second upper). As a negative control, we prepared the wells in which only the OT-II T cells and OVA protein were present without any APCs in the culture (Fig. 4a, bottom). The results indicated that although CD11c$^+$ Aire-DCs function as APCs, Aire was not required for this action.

We also examined the Ag-presenting capacity of Aire$^+$ BMDCs. We mixed CFSE-labeled transgenic OT-II T cells with AGF$^+$ BMDCs at a 10:1 ratio. When OVA protein was added into the culture raging from 1 to 100 μg/ml, we observed the proliferation of OT-II T cells in a dose-dependent manner (Fig. 4B, top). However, CD11c^{high}MHC-II^{high} BMDCs showing no Aire expression also induced a comparable degree of proliferation of OT-II T cells in the presence of OVA (Fig. 4B, bottom). Similar to the case for CD11c$^+$ Aire-DCs, AGF$^+$ BMDCs lacking functional Aire protein established from homozygous Aire/AGF-KI (KI/KI) also induced the proliferation of OT-II T cells (Fig. 4B, middle). The results indicated that although Aire$^+$ BMDCs function as APCs, Aire was not required for this action as we have seen in the CD11c$^+$ Aire-DCs from the LNs (Fig. 4A).

Cells were gated for the CD45$^+$CD11c$^+$MHC-II^{high} fraction. One representative result from more than three repeats is shown. (**C**) Cervical LNs contained significantly higher percentages of CD11c$^+$ Aire-DCs compared with LNs from the other portions (inguinal and axillary LNs). One dot corresponds to one mouse analyzed (left). ***$p < 0.005$. Cervical LNs contained a lower proportion of the cDC1 type of CD11c$^+$ Aire-DCs compared with other peripheral LNs (right). (**D**) CCR7^{high} migratory DCs showed a slightly higher expression level of MHC-II compared with CCR7^{low} resident DCs whereas CCR7^{high} migratory DCs showed a slightly lower expression of CD11c compared with CCR7^{low} resident DCs. One representative result from more than three repeats is shown. (**E**) Approximately half of the CD11c$^+$ Aire-DCs showed CCR7$^{medium\ to\ high}$ expression (migratory type) and the other half showed CCR7^{low} expression (resident type) (lower left). AGF$^-$ DCs also showed similar compositions of migratory and resident types of DCs (lower right). One dot corresponds to one mouse analyzed, and one representative FACS profile is shown (upper). (**F**) Expression of the molecules related to the Ag presentation (upper) and the markers for eTACs (lower) was evaluated for CD11c$^+$ Aire-DCs (in red) and AGF$^-$ DCs (in blue). Cells were gated for the CD45$^+$CD11c$^+$MHC-II^{high} fraction as shown in (A). Total BM cells served as control (in gray). One representative result from more than three repeats is shown.

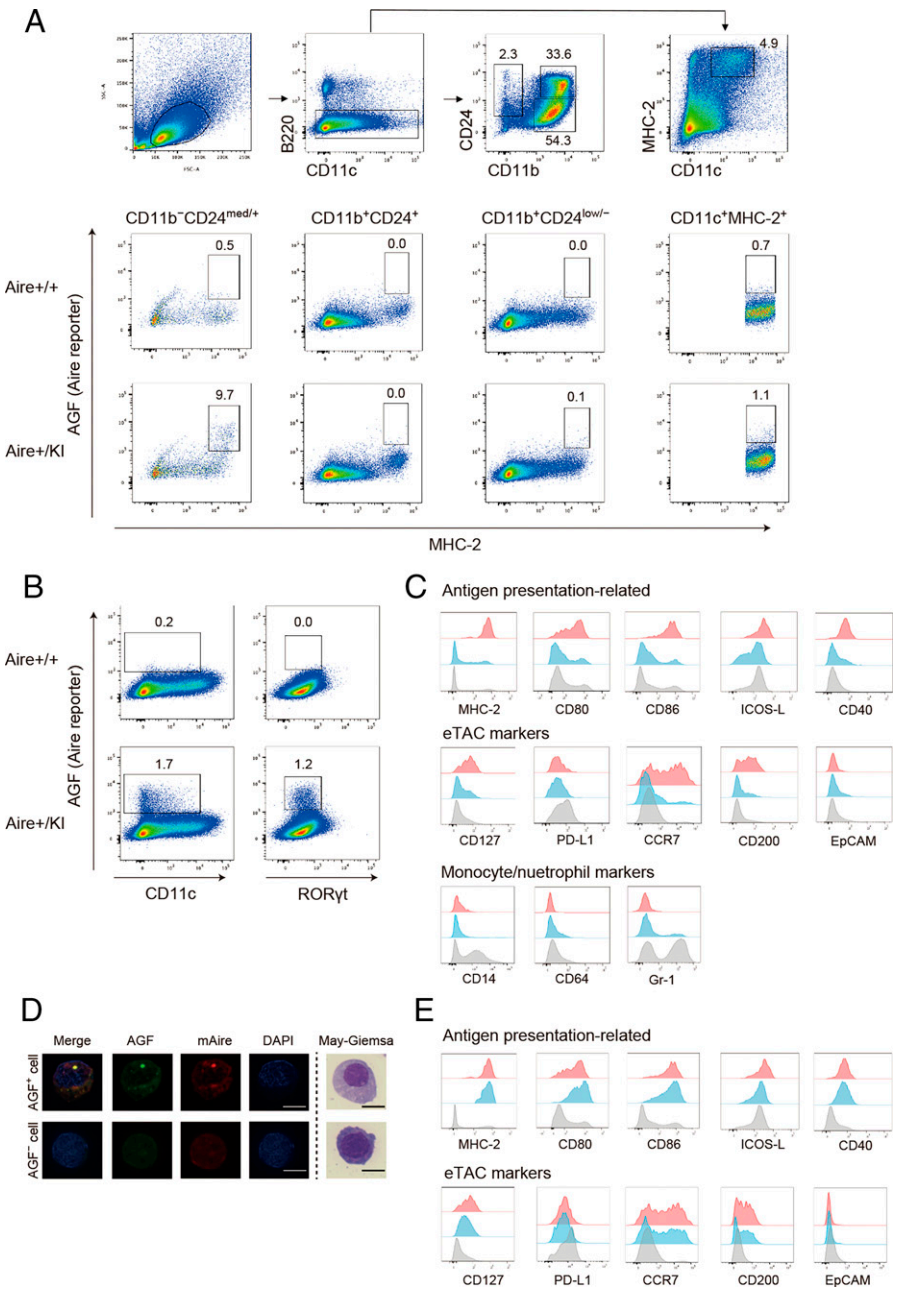

FIGURE 3. In vitro induction of Aire-expressing DCs from the BM.

(**A**) BM cells were cultured with GM-CSF and IL-4, and B220$^-$ cells were divided into CD11b$^-$CD24$^{med/+}$, CD11b$^+$CD24$^+$, and CD11b$^+$CD24$^{low/-}$ (top, second right), and their expression of AGF and MHC-II were evaluated. A CD11c^{high}MHC-II^{high} fraction from B220$^-$ cells was also evaluated for the expression of AGF and MHC-II (top, most right). The CD11c^{high}MHC-II^{high} fraction served as Aire$^-$ BMDCs. One representative result from more than three repeats is shown. (**B**) Expression of CD11c and RORγt together with AGF from BM cells cultured with GM-CSF and IL-4. Cells were gated for lineage$^-$ (CD3, CD19, B220, and Gr-1) cells. One representative result from more than three repeats is shown. (**C**) Expression of the molecules related to the Ag presentation (top), markers for eTACs (middle), and markers for monocytes/neutrophils (bottom) was evaluated for AGF$^+$ BMDCs (in red) and AGF$^-$ BMDCs (in blue). Cells were gated for the B220$^-$CD11b$^-$CD24$^{med/+}$ fraction as shown in (A). Total BM cells served as control (in gray). One representative result from more than three repeats is shown. (**D**) Expression of Aire protein from AGF$^+$ BMDCs (upper) and AGF$^-$ BMDCs for control (lower). Cells were stained with anti-GFP and anti-Aire Abs. Nuclei were stained with DAPI. May–Giemsa solution was used for the counterstaining. Scale bars, 10 μm. One representative result from more than three repeats is shown. (**E**) Expression of the molecules related to the Ag presentation (upper) and markers for eTACs (lower) was evaluated for Aire-sufficient AGF$^+$ BMDCs established from Aire/AGF-KI (+/KI) (in red) and Aire-deficient Aire/AGF-KI (KI/KI) (in blue). Total BM cells served as control (in gray). AGF$^+$ BMDCs were gated for B220$^-$CD11b$^-$CD24$^{med/+}$ fraction as shown in (A). One representative result from more than three repeats is shown.

Dispensable role of Aire in induction of the Th17 response against C. albicans

It has been recently demonstrated that RORγt$^+$ Aire-APCs play important roles in the protection against *C. albicans* through eliciting the Th17-mediated immune response, and Aire in RORγt$^+$ Aire-APCs is indispensable for this action (15). We therefore asked whether Aire in CD11c$^+$ Aire-DCs has a similar role. We first confirmed that Aire plays an important role in the host defense against *C. albicans* using the mouse model on a C57BL/6 background. When the mouths of the animals were swabbed with live *C. albicans* (26), Aire-KO showed higher clinical scores compared with WT mice (Supplemental Fig. 2A, 2B). CFU from the tongues (Supplemental Fig. 2C) and histological scores (Supplemental Fig. 2D, 2E) were also higher in Aire-KO compared with WT mice. The results indicated that Aire-KO on a C57BL/6 background is suitable for the assessment of the host defense against *C. albicans*. To address whether higher susceptibility to oral infection of *C. albicans* in Aire-KO involves any role of Aire in the CD11c$^+$ Aire-DCs, mice were in vivo primed by an MP fraction of mycelial cells of *C. albicans* (26) with CFA injected s.c. Six days later, CD4$^+$ T cells were isolated from the LNs and spleen. CD4$^+$ T cells primed by s.c. injection of the MP fraction of mycelial cells were then cocultured with CD11c$^+$ Aire-DCs from heterozygous Aire/AGF-KI.

https://doi.org/10.4049/immunohorizons.2200103

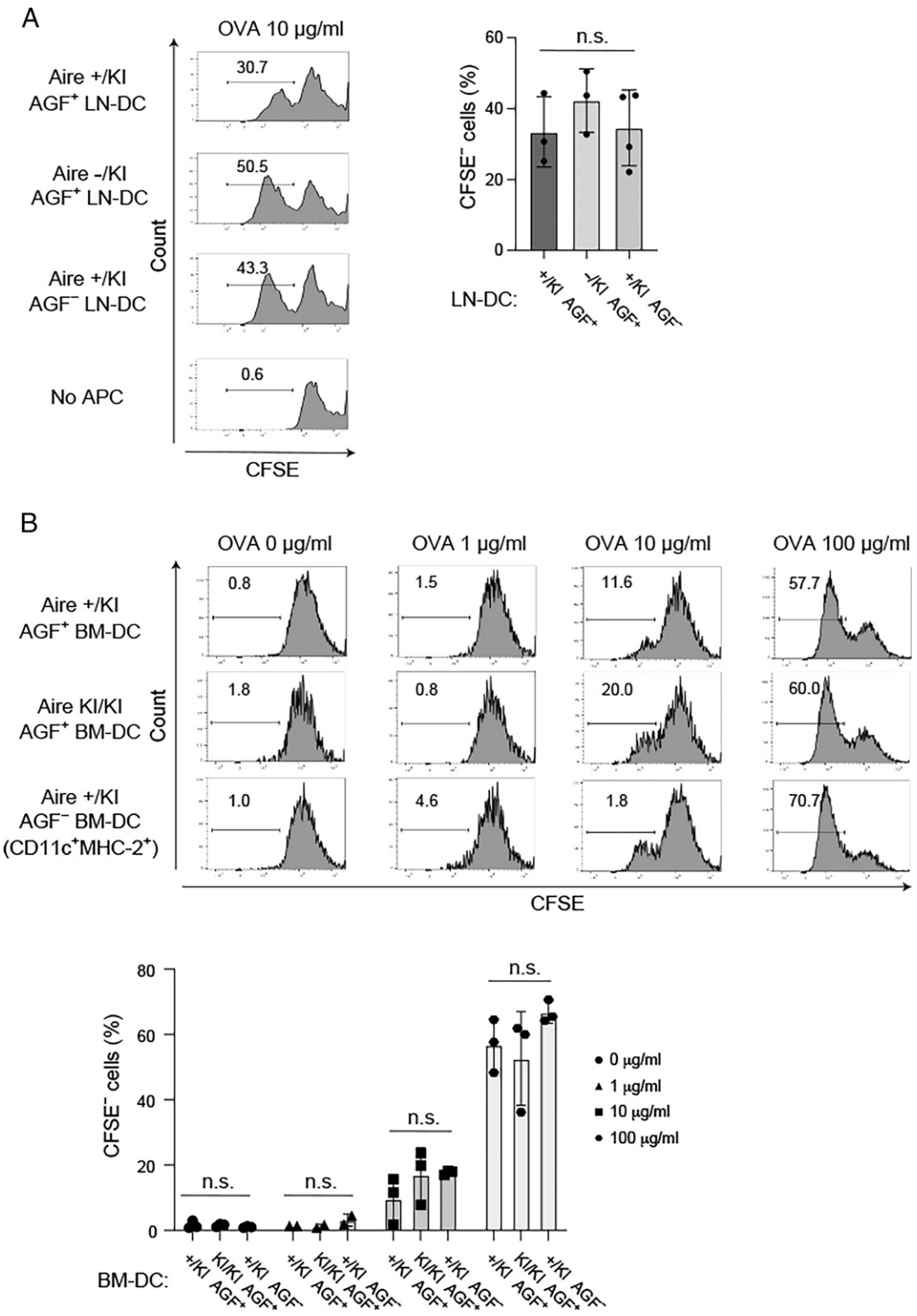

FIGURE 4. The Ag-presenting capacity of CD11c$^+$ Aire-DCs. (**A**) CFSE-labeled CD4$^+$ OT-II T cells were cocultured with AGF$^+$CD11c$^+$ LN-DCs, Aire$^{less\text{-}AGF}$ CD11c$^+$ LN-DCs (Aire deficient), or AGF$^-$CD11c$^+$ LN-DCs in the presence of OVA protein (10 μg/ml) for 3 d. Percentages of CFSE$^-$CD4$^+$ OT-II T cells were measured by flow cytometry. One representative FACS profile of more than three repeats is shown on the left. A summary of the results is shown on the right. One dot corresponds to one mouse analyzed, and the bars indicate means ± SD. n.s., not significant. (**B**) CFSE-labeled CD4$^+$ OT-II T cells were cocultured with AGF$^+$ BMDCs from Aire/AGF-KI (+/KI), Aire$^{less\text{-}AGF}$ BMDCs from Aire/AGF-KI (KI/KI) (Aire deficient), or CD11c^{high}MHC-II^{high} BM-DCs (AGF$^-$ BMDCs from Aire/AGF-KI (+/KI)) in the presence of various concentrations of OVA protein for 3 d. Percentages of CFSE$^-$CD4$^+$ OT-II T cells were measured by flow cytometry. One representative FACS profile of more than three repeats is shown in the upper panel. A summary of the results is shown in the lower panel. One mark corresponds to one mouse analyzed, and the bars indicate means ± SD. n.s., not significant.

Significant induction of CD4$^+$ Th17 cells was observed only in the presence of the recall Ag during the culture (Fig. 5A, 5B). Of note, when the primed CD4$^+$ T cells were cocultured with CD11c$^+$AGF$^+$ DCs isolated from homozygous Aire/AGF-KI in which there is no functional Aire protein, we also observed similar induction of CD4$^+$ Th17 cells (Fig. 5B, 5D). Thus, CD11c$^+$ Aire-DCs could function as APCs in the induction of the Th17-mediated immune response against *C. albicans*, and Aire in

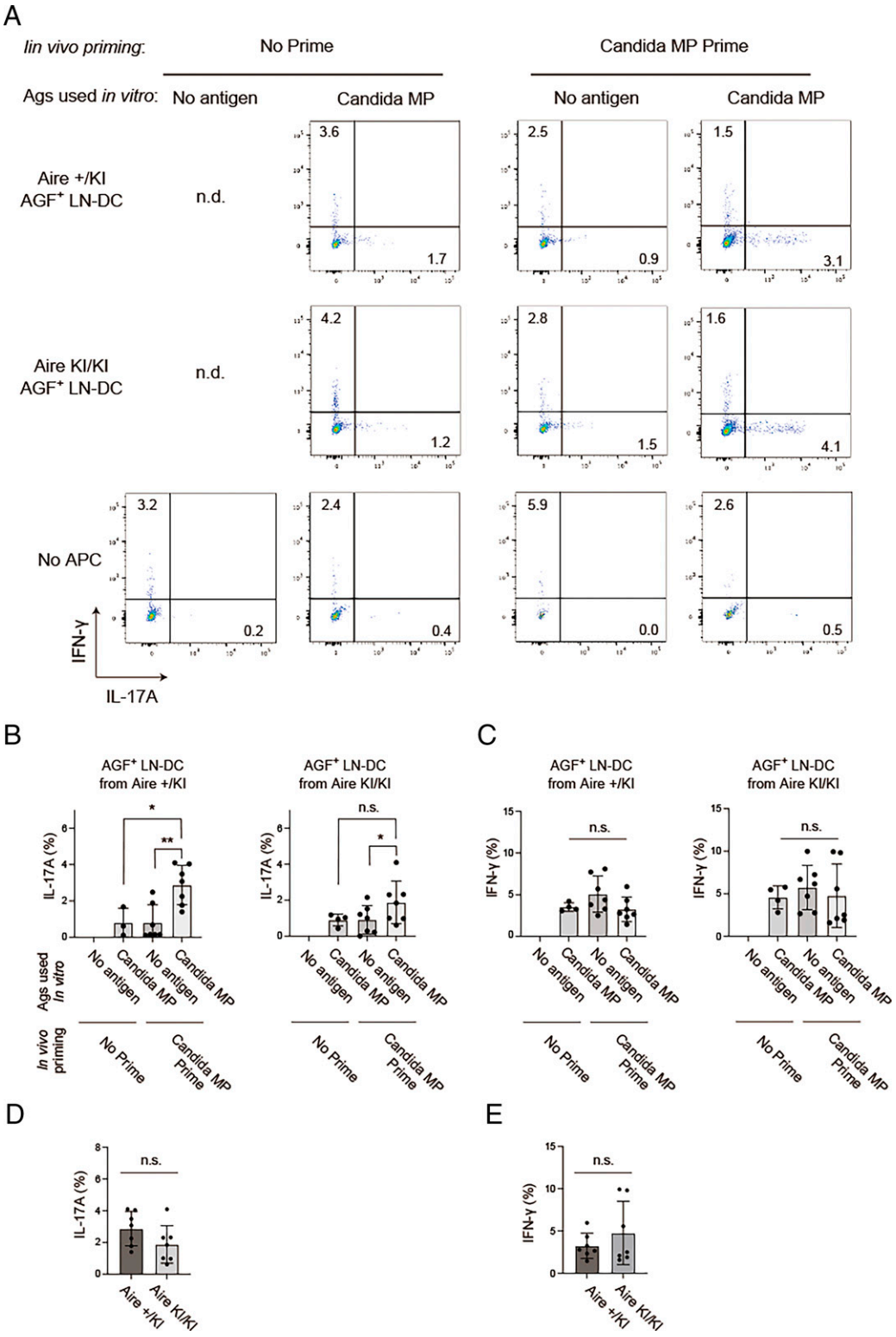

FIGURE 5. Dispensable role of Aire in Aire$^+$ LN-DCs in induction of the Th17 response against *C. albicans*.

(**A**) CD4$^+$ T cells isolated from WT mice injected s.c. with the MP fraction of *C. albicans* mycelial cells or PBS were cocultured with AGF$^+$ CD11c$^+$ LN-DCs from heterozygous Aire/AGF-KI (top) and Aire$^{less\text{-}AGF}$ CD11c$^+$ LN-DCs from homozygous Aire/AGF-KI (middle) in the presence or absence of recall Ag (MP fraction of *C. albicans* mycelial cells) for 6 d. Production of IL-17A and IFN-γ in CD4$^+$ T cells was analyzed by flow cytometry. CD4$^+$ T cells cocultured without APCs served as negative control (No APC: bottom). One representative FACS profile of more than three repeats is shown. n.d., not determined. (**B** and **C**) Summary of the results of the percentage of IL-17A$^+$CD4$^+$ T cells (B) and IFN-γ$^+$ CD4$^+$ T cells (C) from in vivo Ag-challenged (*Candida* MP primed) or control mice (not primed) cultured with (*Candida* MP) or without recall Ags (no Ag) in vitro. One dot corresponds to one mouse analyzed, and the bars indicate means ± SD. *$p < 0.05$, **$p < 0.01$; n.s., not significant. (**D** and **E**) Comparison of the percentage of IL-17A$^+$CD4$^+$ T cells (D) and IFN-γ$^+$CD4$^+$ T cells (E) from in vivo Ag-challenged mice (Candida MP primed) cultured with recall Ags (*Candida* MP) in vitro shown in (B) and (C), respectively. The results were compared between Aire-sufficient (+/KI) and Aire-deficient mice (KI/KI). n.s., not significant.

CD11c$^+$ Aire-DCs was not required for this action. This result was in great contrast to the role of Aire in RORγt$^+$ Aire-APCs (15). Interestingly, we also observed the induction of CD4$^+$ Th17 cells even when we used Aire-nonexpressing CD11c$^+$ AGF$^-$ DCs from both heterozygous and homozygous Aire/AGF-KI (Supplemental Fig. 3A, 3B, 3D). The results suggested that the ability to induce *C. albicans*–specific Th17 immune response may not be confined to Aire$^+$ DCs among cDCs.

https://doi.org/10.4049/immunohorizons.2200103

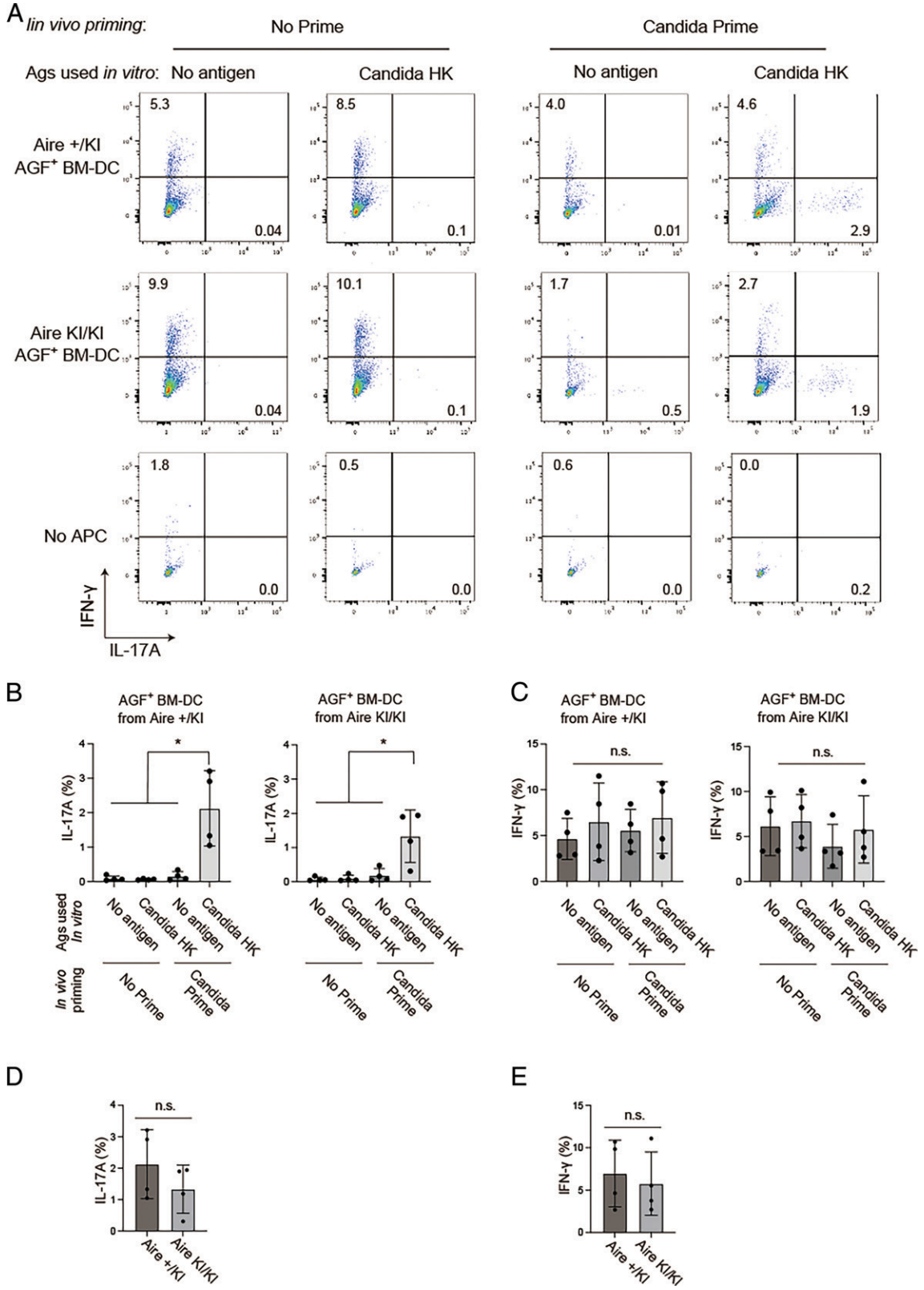

FIGURE 6. Dispensable role of Aire in Aire$^+$ BMDCs in induction of the Th17 response against *C. albicans*.

(**A**) CD4$^+$ T cells isolated from WT mice primed by an intragastric injection of live *C. albicans* or PBS were cocultured with AGF$^+$ BMDCs from Aire-sufficient (+/KI, top) and Aire$^{less\text{-}AGF}$ BM-DCs from Aire-deficient backgrounds (KI/KI, middle) in the presence or absence of recall Ag (heat-killed [HK] *C. albicans*) for 6 d. Production of IL-17A and IFN-γ in CD4$^+$ T cells was analyzed by flow cytometry. CD4$^+$ T cells cocultured ***(Continued)***

We also examined the role of Aire in induction of the *C. albicans*–specific Th17 immune response using Aire$^+$ BMDCs. In this case, mice were primed with an intragastric injection of live *C. albicans* (26). Ten days later, CD4$^+$ T cells primed with live *C. albicans* were isolated from the LNs and spleen, and they were cocultured with Aire$^+$ BMDCs in the presence of heat-killed *C. albicans*. We observed higher induction of CD4$^+$ Th17 cells in the presence of recall Ag compared with no recall Ag during the culture on Aire-sufficient background (+/KI; Fig. 6A, 6B). The Th17 response was observed only when mice were primed with live *C. albicans*, indicating that Aire$^+$ BMDCs could elicit the *C. albicans*–specific adoptive Th17 immune response in this model. We then examined whether AGF$^+$ BMDCs isolated from homozygous Aire/AGF-KI in which there is no functional Aire protein could induce a CD4$^+$ Th17 response. We observed similar induction of CD4$^+$ Th17 cells even when AGF$^+$ BMDCs lacked functional Aire protein (KI/KI; Fig. 6B, 6D). The results indicated that Aire in AGF$^+$ BMDCs was not required for this action as we have seen in the experiments using CD11c$^+$ Aire-DCs. In contrast, we did not see any significant induction of CD4$^+$ Th1 cells against *C. albicans* in this protocol (Figs. 5C, 5E, 6C, 6E, Supplemental Fig. 3C, 3E).

Role of Aire in the production of the transcriptome of CD11c$^+$ Aire-DCs

The data so far indicated that CD11c$^+$ Aire-DCs isolated from LNs as well as the cultured Aire$^+$ BMDCs could function as efficient APCs. In contrast, we noticed that Aire itself was not required for these actions. Given that Aire plays an important role in shaping the transcriptome in mTECs, we next examined the role of Aire in the production of transcriptome within CD11c$^+$ Aire-DCs. We isolated CD45$^+$CD11c$^+$MHC-II$^+$ cells from the LN suspensions using Aire-sufficient (+/KI) and Aire-deficient mice (−/KI) and divided them into the AGF$^+$ and AGF$^-$ fractions. In this study, the AGF$^+$ fraction from CD45$^+$CD11c$^+$MHC-II$^+$ cells corresponded to CD11c$^+$ Aire-DCs but not to RORγt$^+$ Aire-APCs because we gated for CD11c$^+$ cells for the isolation. We prepared Aire$^+$ BMDCs on both Aire-sufficient (+/KI) and Aire-deficient backgrounds (−/KI) for investigating their transcriptomes (GSE211006). When the transcriptomes from CD11c$^+$ Aire-DCs, Aire (AGF)$^-$ DCs, Aire$^+$ BMDCs, and mTEC^{high} on both Aire-sufficient and Aire-deficient backgrounds were compared, there was much difference between eTACs (CD11c$^+$ Aire-DCs and Aire$^+$ BM-DCs) and mTEC^{high} (Fig. 7A). Indeed, the transcriptome from Aire$^+$ BMDCs was closer to that from the CD11c$^+$ Aire-DCs compared with that from mTEC^{high} irrespective of the presence or absence of Aire by the principal component analysis (Supplemental Fig. 4A). We compared the expression levels of Aire between eTACs and mTEC^{high} and found that eTACs expressed Aire as low as one-seventh to one-eighth of mTECs by trimmed mean of M value (TMM) normalized counts (Fig. 7A, upper columns). Of note, we did not observe major changes in the transcriptome in DCs even in the absence of Aire unlike in the case of mTECs (Fig. 7A, lower heatmap).

When the transcriptome from AGF$^+$ cells (from +/KI) and that from Aire$^{less\text{-}AGF}$ cells (from −/KI) were compared in CD11c$^+$ Aire-DCs, we found that *Aire* and *Fn1* were upregulated whereas *Dnmt3l* was downregulated, and no other genes were significantly changed among 15,037 genes detected (fold change >2 or <0.5; false discovery rate [FDR] <0.05) (Fig. 7B, left). In this case, alteration in the expression of *Aire* and *Dnmt3l* was due to the gene-targeting event, and *Fn1* was the only bona fide differentially expressed gene. Similarly, when we compared the transcriptome between Aire$^+$ BMDCs and Aire$^{less\text{-}AGF}$ BMDCs, *Aire* and *Dnmt3l* were the only genes that showed significant alteration (Fig. 7B, right). Thus, Aire deficiency did not affect the gene expression profiles in both CD11c$^+$ Aire-DCs from LNs and cultured Aire$^+$ BMDCs. When we applied Aire-dependent genes extracted from mTEC^{high} (WT versus Aire-KO, fold-change >2 and FDR <0.05) to the transcriptome of CD11c$^+$ Aire-DCs, we observed no difference in their distribution from all the other genes (Fig. 7C, Supplemental Fig. 4B: Wilcoxon rank sum test p value = 0.1683 and χ^2 test p value = 0.2531, respectively). The results indicated that Aire-dependent genes in mTEC^{high} were not Aire-dependent in CD11c$^+$ Aire-DCs.

To compare the role of Aire in gene control in CD11c$^+$ Aire-DCs with that in mTECs more globally, we examined the correlation of Aire dependency defined by the fold change–fold change plot between CD11c$^+$ Aire-DCs and mTEC^{high}. No significant correlation was found between CD11c$^+$ Aire-DCs and mTECs in their gene expression induced by Aire (Fig. 7D, left). Because Aire in mTECs controls the transcriptome of TRAs for self-tolerance, we also focused on the expression of TRAs from CD11c$^+$ Aire-DCs. We found that only a single TRA gene, *Fn1*, was significantly upregulated (fold-change >2 and FDR <0.05) in AGF$^+$ cells compared with Aire$^{less\text{-}AGF}$ cells for CD11c$^+$ Aire-DCs (Fig. 7D, right). In contrast, the expression of TRAs from mTEC^{high} was dramatically up regulated (fold change >2 and FDR <0.05) in the presence of Aire (Fig. 7D, right), and there was no overlap with the TRA genes upregulated in CD11c$^+$

without APCs served as negative control (No APC: bottom). One representative FACS profile of more than three repeats is shown. (**B** and **C**) Summary of the results of the percentage of IL-17A$^+$CD4$^+$ T cells (B) and IFN-γ$^+$CD4$^+$ T cells (C) from in vivo Ag-challenged (live *Candida* primed) or control mice (not primed) cultured with (HK *Candida*) or without recall Ags (no Ag) in vitro. One dot corresponds to one mouse analyzed, and the bars indicate means ± SD. *$p < 0.05$, n.s., not significant. (**D** and **E**) Comparison of the percentage of IL-17A$^+$CD4$^+$ T cells (D) and IFN-γ$^+$CD4$^+$ T cells (E) from in vivo Ag-challenged mice (live *Candida* primed) cultured with recall Ags (HK *Candida*) in vitro shown in (B) and (C), respectively. The results were compared between Aire-sufficient (+/KI) and Aire-deficient mice (KI/KI). n.s., not significant.

https://doi.org/10.4049/immunohorizons.2200103

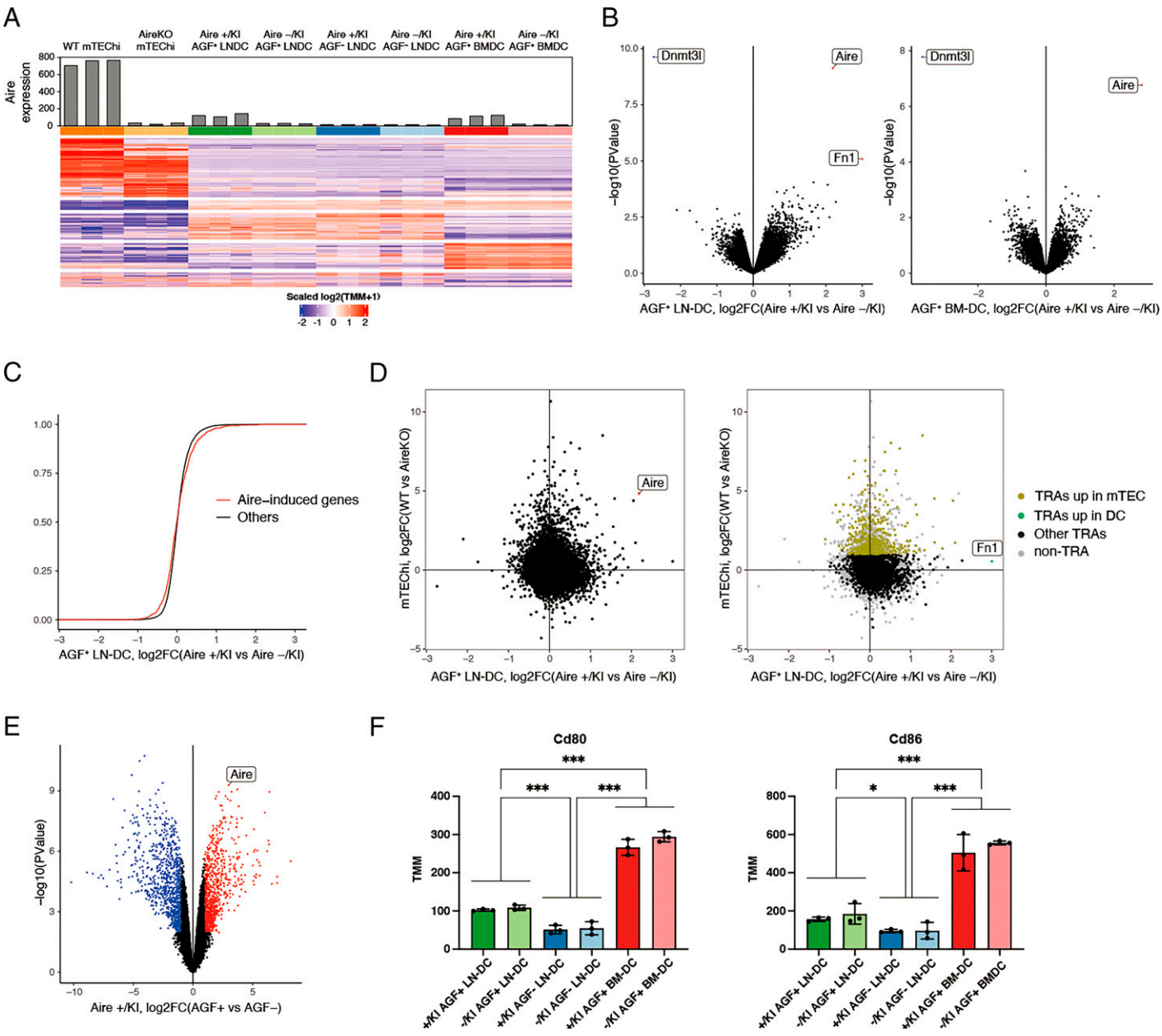

FIGURE 7. Role of Aire in the production of the transcriptome of CD11c$^+$ Aire-DCs.

(**A**) Heatmap visualization comparing the transcriptome (a total of 20,330 genes) from mTEC^{high}, AGF$^+$ LN-DCs (CD11c$^+$ Aire-DCs), AGF$^-$ LN-DCs, and AGF$^+$ BMDCs on Aire-sufficient (+/KI) and Aire-deficient backgrounds (−/KI) for each (from left to right). The gene list (row of the heatmap) was separated into five categories: genes characteristic for mTEC^{high} (top), genes common to DCs (second from the top), genes characteristic for LN-DCs (middle), genes characteristic for BMDCs (second from the bottom), and other genes (bottom). For mTEC^{high}, the RNA-seq data of three representative replicates are shown for each genotype. The bar plot above the heatmap represents the expression level of Aire (TMM normalized counts) for each sample. (**B**) Volcano plot comparing the transcriptome between AGF$^+$CD11c$^+$ Aire-DCs from Aire-sufficient (+/KI) and Aire$^{less\text{-}AGF}$ CD11c$^+$ Aire-DCs from Aire-deficient (−/KI) (left). Volcano plot comparing the transcriptome between Aire$^+$ BMDCs from Aire-sufficient (+/KI) and Aire$^{less\text{-}AGF}$ BMDCs from Aire-deficient (−/KI) (right). Three independent biological replicates from each genotype were used for RNA-seq analysis. Genes statistically upregulated (fold change >2 and FDR <0.05) (*Aire* and *Fn1*) and downregulated (fold change <0.5 and FDR <0.05) (*Dnmt3l*) are indicated. (**C**) Cumulative distribution plot for Aire-dependent genes (1,072 genes detected in DCs) and other genes (13,965 genes), presented as the cumulative probability for the $\log_2$ (fold change) of the expression value between AGF$^+$CD11c$^+$ Aire-DCs from Aire-sufficient (+/KI) and Aire$^{less\text{-}AGF}$CD11c$^+$ Aire-DCs from Aire-deficient (−/KI). (**D**) Scatter plot of the fold change between AGF$^+$CD11c$^+$ Aire-DCs from Aire-sufficient (+/KI) and Aire$^{less\text{-}AGF}$CD11c$^+$ Aire-DCs from Aire-deficient (−/KI) (*x*-axis) versus the fold change between mTEC^{high} from WT and mTEC^{high} from Aire-KO (*y*-axis) (left). TRA genes upregulated in mTEC, TRA genes upregulated in DCs, other TRA genes, and non-TRA genes included **(*Continued*)**

Aire-DCs. Thus, Aire in CD11c$^+$ Aire-DCs does not have a major impact on the production of the transcriptome including that for TRAs, unlike Aire in mTECs.

Given that loss of Aire in CD11c$^+$ Aire-DCs showed no clear alterations in the Ag-presenting capacity for exogenous Ags (i.e., OVA and *C. albicans*) as well as in the production of the transcriptome, we investigated the identity of CD11c$^+$ Aire-DCs by comparing the transcriptome between AGF$^+$CD11c$^+$ Aire-DCs and Aire (AGF)$^-$ DCs. We observed 810 upregulated (fold change >2 and FDR <0.05) and 858 downregulated (fold change <0.5 and FDR <0.05) genes from CD11c$^+$ Aire-DCs when compared with those from Aire$^-$ DCs on an Aire-sufficient background (Fig. 7E). Rather unexpectedly, GO analysis of the upregulated genes in CD11c$^+$ Aire-DCs showed the terms mostly related to the cellular development and general function rather than the immunological function (Supplemental Fig. 4C, left). Conversely, GO terms associated with immunological function were entirely enriched in Aire$^-$ DCs (Supplemental Fig. 4C, right). Consistent with this finding, gene set enrichment analysis confirmed that genes belonging to the GO term "activation of immune response" were upregulated in Aire$^-$ DCs (Supplemental Fig. 4D). The same transcriptomic changes between AGF$^+$CD11c$^+$ Aire-DCs and Aire$^-$ DCs were observed even on an Aire-deficient background (Supplemental Fig. 4E). In contrast, expression levels of costimulatory molecules such as *Cd80* and *Cd86* were higher in AGF$^+$CD11c$^+$ Aire-DCs compared with Aire$^-$ DCs (Fig. 7F), consistent with the results of flow cytometric analysis at least for CD86 (Fig. 2F, upper). Furthermore, the expression of costimulatory molecules was higher in Aire$^+$ BMDCs compared with Aire$^-$ BMDCs, consistent with the flow cytometric analysis (Fig. 3C). The results suggested that Aire-DCs are in the "mature" stage characterized by the high expression of *Cd80* and *Cd86*, whereas genes related to immunogenic GO were more prominent in Aire$^-$ DCs. The fact that the expression of Aire and the identity of CD11c$^+$ Aire-DCs were not linked, as exemplified by the results shown in Supplemental Fig. 4E, may strengthen our conclusion on the dispensable role of Aire in CD11c$^+$ Aire-DCs from a different aspect. Finally, we found that Aire$^+$ BMDCs showed high expression of genes related to the cell cycle (Supplemental Fig. 4F), probably due to the massive expansion upon supplementation with cytokines.

DISCUSSION

A recent detailed single-cell multiomics approach has clearly demonstrated that there are two classes of eTACs (11): migratory DC-type eTACs and ILC3-like eTACs expressing RORγt (10). We have confirmed the presence of two types of Aire-expressing APCs in the periphery, cDC-type eTACs and ILC3-like–type eTACs, using a high-fidelity Aire-reporter mouse strain coupled with conventional flow cytometric and immunohistochemical analyses. These two types of eTACs showed different expression levels of Aire and a distinct location in the LNs. Although the single-cell multiomics approach has suggested that both classes of eTACs are DCs, and that migratory DC-type eTACs have the characteristics of migratory DCs with high CCR7 expression (11), our flow cytometric analysis has revealed that CD11c$^+$ Aire-DCs were not confined to the migratory DCs. Instead, CD11c$^+$ Aire-DCs were composed of both CCR7^{high} migratory DCs and CCR7^{low} resident DCs at a roughly equal ratio (Fig. 2E) (39, 40). We therefore classified Aire$^+$ DCs into the cDC-type Aire$^+$ cells (cDC-type eTACs) and ILC3-like–type Aire$^+$ cells (ILC3-like–type eTACs) in this study. One possible reason for the phenotypic difference between our study and the single-cell multiomics study might originate from the different Aire-reporter strains used: the straight KI of the Aire-reporter molecule in our study (16) versus BAC transgenic mice in the other study (11). The difference in the form of reporter molecules for cell sorting (authentic Aire-GFP nuclear dots in our study versus GFP from the whole cell in the other study) might be another possible reason for the discrepancy.

Although the indispensable role of Aire in ILC3-like–type eTACs in the control of *C. albicans* was clearly demonstrated in the recent report (15), the exact role of Aire in cDC-type eTACs in the Ag presentation and production of the transcriptome has not been investigated until the current study. So far, we found that Aire in cDC-type eTACs has no major impact on the Ag-presenting capacity for protein Ag (OVA) as well as for the infectious agent of *C. albicans*. Given that more CD11c$^+$ Aire-DCs were present in the cervical LNs (in which the immune response against oral and esophageal candidiasis might be taking place) than in other peripheral LNs, this was further unexpected for the following reasons. First, cDC-type eTACs dominated ILC3-like–type eTACs in number by several fold, although the expression level of Aire from each cell in cDC-type eTACs was lower compared with that from ILC3-like–type eTACs. Second, cDC-type eTACs were predominantly located in the T cell areas within LNs where Ag-specific T cells should have better access to APCs (Fig. 1F). In contrast, ILC3-like–type eTACs were mainly located in the interfollicular spaces of the B cells where interaction with T cells in situ may not be so frequent at least at a steady state. Therefore, higher expression of *C. albicans*–sensing receptors such as Galectin-3, Dectin-1, and TLR2 from

in the scatter plot (left) are distinguished by the color on the right. (**E**) Volcano plot comparing the transcriptome between AGF$^+$CD11c$^+$ Aire-DCs and AGF$^-$CD11c$^+$ DCs both from Aire-sufficient (+/KI). Three independent biological replicates from each genotype were used for RNA-seq analysis. Statistically upregulated (fold change >2 and FDR <0.05) and downregulated genes (fold change <0.5 and FDR <0.05) are highlighted in red and blue, respectively. (**F**) Expression level (TMM normalized counts) of *Cd80* and *Cd86* in each sample. One dot corresponds to one mouse analyzed. *$p < 0.05$, ***$p < 0.005$.

https://doi.org/10.4049/immunohorizons.2200103

ILC3-like–type eTACs (15) might have overcome their quantitative and anatomical disadvantages for the immune response against *C. albicans*. Indeed, transcriptomic analyses of ILC3-like–type eTACs between WT and Aire-KO were performed after repeated challenges with heat-killed *C. albicans* (15), and Aire-dependent expression of cell adhesion molecules, costimulatory molecules, and proinflammatory responses might have together contributed to the host defense by the ILC3-like–type eTACs upon *Candida* infection. In this regard, unidentified immune functions of cDC-type eTACs by employing different experimental models may be required. Furthermore, elucidation of the distinct role of cDC-type eTACs and ILC3-like–type eTACs beyond the host defense against *C. albicans* will help our better understanding of the Aire-mediated immune homeostasis in the periphery.

For the assessment of the immune response against *C. albicans*, we have used the MP fraction of mycelial cells from *C. albicans* in some experiments because mice primed with this fraction promoted the differentiation of $CD4^+$ T cells into Th17 (26). Furthermore, Th17 cells differentiated in response to this fraction could prevent murine oral candidiasis. Although we could induce the immune response against *C. albicans* using cDC-type eTACs with this *Candida* MP Ag, we observed no major role of Aire in cDC-type eTACs for this action. We speculate that Aire in ILC3-like–type eTACs plays a role in shaping the unique function of this population through capturing and presenting Ags from *C. albicans* in an Aire-dependent manner. This protective function of ILC3-like–type eTACs was not compensated by the cDC-type eTACs. Accordingly, identifying the effective T cell Ags from *C. albicans* presented by ILC3-like–type eTACs is an important issue to develop effective immunotherapy against candidiasis. Nevertheless, whether Aire-mediated thymic tolerance is additionally contributing to the host defense against *C. albicans* requires further study. This is because Aire deficiency results in the production of neutralizing autoantibodies against IL-17A, IL-17F, and IL-22, which also play a role during the *Candida* infection (43, 44). Conversely, whether ILC3-like–type eTACs are involved in peripheral self-tolerance besides the protection against *C. albicans* is another interesting question. Interestingly, ILC3-like–type eTACs showed the transcriptional and regulatory homology to mTECs revealed by single-cell multiomics (11).

eTACs have been originally demonstrated to express a diverse array of distinct self-antigens, the spectrum of which is complementing those of mTECs (9). eTACs are capable of interacting with and deleting naive autoreactive T cells (9) or inactivating cognate T cells (45), a seemingly analogous way by which $Aire^+$ mTECs contribute to thymic self-tolerance. Importantly, however, note that the tolerogenic role of eTACs has been demonstrated by the transgenic mouse models: pancreatic self-antigens (i.e., BDC2.5 [45], hybrid peptides between chromogranin A and insulin [46], and islet-specific glucose-6-phosphatase catalytic subunit-related protein (IGRP) [11]) were driven by the Aire promoter in these animal models. By crossing with corresponding TCR-transgenic mice, the authors demonstrated that the presentation of the model self-antigens from the eTACs was relevant to the control of diabetes development. Although these studies suggested the significance of the expression of self-antigens from eTACs, the outcome of Aire deficiency in eTACs has not been tested. Similarly, although eTACs have been demonstrated to play a role in maternal–fetal tolerance (47), the study was performed by the ablation of eTACs using Aire-promotor–driven diphtheria toxin receptor coupled with diphtheria toxin injection. Thus, although eTACs may constitute an important component of peripheral self-tolerance, the central question remains unanswered of whether Aire has any cell-intrinsic role in the function of eTACs for establishing self-tolerance. Further work is required to answer this question by comparing the cellular heterogeneity between WT and Aire-KO at a single-cell level (48).

So far, we have no evidence for the functional importance of Aire in cDC-type eTACs for Ag presentation and the production of the transcriptome. In this regard, one study characterizing the eTACs from human tonsils merits attention (41). The study concluded that the expression of Aire was transient, rather than stable, and was associated with the differentiation to a mature phenotype of eTACs. The study also concluded that Aire expression within eTACs was not associated with an enriched expression of TRAs. Based on the results of our present study, we favor this notion. In this case, the expression of Aire might be a bystander phenomenon during the differentiation into mature DCs rather than Aire being responsible for acquiring the capacity for Ag presentation in cDC-type eTACs. Alternatively, antigenic stimuli may change the significance of Aire in cDC-type eTACs that were not tested in our work. The relative importance between cDC-type eTACs and ILC3-like–type eTACs in immune control under various conditions needs further study.

DISCLOSURES

The authors have no financial conflicts of interest.

REFERENCES

1. Kadouri, N., S. Nevo, Y. Goldfarb, and J. Abramson. 2020. Thymic epithelial cell heterogeneity: TEC by TEC. *Nat. Rev. Immunol.* 20: 239–253.
2. Kisand, K., and P. Peterson. 2011. Autoimmune polyendocrinopathy candidiasis ectodermal dystrophy: known and novel aspects of the syndrome. *Ann. N. Y. Acad. Sci.* 1246: 77–91.
3. Mathis, D., and C. Benoist. 2009. Aire. *Annu. Rev. Immunol.* 27: 287–312.
4. Březina, J., M. Vobořil, and D. Filipp. 2022. Mechanisms of direct and indirect presentation of self-antigens in the thymus. *Front. Immunol.* 13: 926625.
5. Anderson, M. S., E. S. Venanzi, Z. Chen, S. P. Berzins, C. Benoist, and D. Mathis. 2005. The cellular mechanism of Aire control of T cell tolerance. *Immunity* 23: 227–239.

6. Anderson, M. S., E. S. Venanzi, L. Klein, Z. Chen, S. P. Berzins, S. J. Turley, H. von Boehmer, R. Bronson, A. Dierich, C. Benoist, and D. Mathis. 2002. Projection of an immunological self shadow within the thymus by the Aire protein. *Science* 298: 1395–1401.
7. Liston, A., S. Lesage, J. Wilson, L. Peltonen, and C. C. Goodnow. 2003. Aire regulates negative selection of organ-specific T cells. *Nat. Immunol.* 4: 350–354.
8. Yang, S., N. Fujikado, D. Kolodin, C. Benoist, and D. Mathis. 2015. Regulatory T cells generated early in life play a distinct role in maintaining self-tolerance. *Science* 348: 589–594.
9. Gardner, J. M., J. J. Devoss, R. S. Friedman, D. J. Wong, Y. X. Tan, X. Zhou, K. P. Johannes, M. A. Su, H. Y. Chang, M. F. Krummel, and M. S. Anderson. 2008. Deletional tolerance mediated by extrathymic Aire-expressing cells. *Science* 321: 843–847.
10. Yamano, T., J. Dobeš, M. Voboril, M. Steinert, T. Brabec, N. Zietara, M. Dobešová, C. Ohnmacht, M. Laan, P. Peterson, et al. 2019. Aire-expressing ILC3-like cells in the lymph node display potent APC features. *J. Exp. Med.* 216: 1027–1037.
11. Wang, J., C. A. Lareau, J. L. Bautista, A. R. Gupta, K. Sandor, J. Germino, Y. Yin, M. P. Arvedson, G. C. Reeder, N. T. Cramer, et al. 2021. Single-cell multiomics defines tolerogenic extrathymic Aire-expressing populations with unique homology to thymic epithelium. *Sci. Immunol.* 6: eabl5053.
12. Kedmi, R., T. A. Najar, K. R. Mesa, A. Grayson, L. Kroehling, Y. Hao, S. Hao, M. Pokrovskii, M. Xu, J. Talbot, et al. 2022. A RORγt^{+} cell instructs gut microbiota-specific T_{reg} cell differentiation. [Published erratum appears in 2022 *Nature* 610: E7.] *Nature* 610: 737–743.
13. Lyu, M., H. Suzuki, L. Kang, F. Gaspal, W. Zhou, J. Goc, L. Zhou, J. Zhou, W. Zhang, Z. Shen, et alJRI Live Cell Bank. 2022. ILC3s select microbiota-specific regulatory T cells to establish tolerance in the gut. *Nature* 610: 744–751.
14. Akagbosu, B., Z. Tayyebi, G. Shibu, Y. A. Paucar Iza, D. Deep, Y. F. Parisotto, L. Fisher, H. A. Pasolli, V. Thevin, R. Elmentaite, et al. 2022. Novel antigen-presenting cell imparts T_{reg}-dependent tolerance to gut microbiota. *Nature* 610: 752–760.
15. Dobeš, J., O. Ben-Nun, A. Binyamin, L. Stoler-Barak, B. E. Oftedal, Y. Goldfarb, N. Kadouri, Y. Gruper, T. Givony, I. Zalayat, et al. 2022. Extrathymic expression of Aire controls the induction of effective T_H17 cell-mediated immune response to *Candida albicans*. *Nat. Immunol.* 23: 1098–1108.
16. Kawano, H., H. Nishijima, J. Morimoto, F. Hirota, R. Morita, Y. Mouri, Y. Nishioka, and M. Matsumoto. 2015. Aire expression is inherent to most medullary thymic epithelial cells during their differentiation program. *J. Immunol.* 195: 5149–5158.
17. Yano, M., N. Kuroda, H. Han, M. Meguro-Horike, Y. Nishikawa, H. Kiyonari, K. Maemura, Y. Yanagawa, K. Obata, S. Takahashi, et al. 2008. Aire controls the differentiation program of thymic epithelial cells in the medulla for the establishment of self-tolerance. *J. Exp. Med.* 205: 2827–2838.
18. Niki, S., K. Oshikawa, Y. Mouri, F. Hirota, A. Matsushima, M. Yano, H. Han, Y. Bando, K. Izumi, M. Matsumoto, et al. 2006. Alteration of intra-pancreatic target-organ specificity by abrogation of Aire in NOD mice. *J. Clin. Invest.* 116: 1292–1301.
19. Jiang, W., M. S. Anderson, R. Bronson, D. Mathis, and C. Benoist. 2005. Modifier loci condition autoimmunity provoked by Aire deficiency. *J. Exp. Med.* 202: 805–815.
20. Kuroda, N., T. Mitani, N. Takeda, N. Ishimaru, R. Arakaki, Y. Hayashi, Y. Bando, K. Izumi, T. Takahashi, T. Nomura, et al. 2005. Development of autoimmunity against transcriptionally unrepressed target antigen in the thymus of Aire-deficient mice. *J. Immunol.* 174: 1862–1870.
21. Matsumoto, M., K. Tsuneyama, J. Morimoto, K. Hosomichi, M. Matsumoto, and H. Nishijima. 2020. Tissue-specific autoimmunity controlled by Aire in thymic and peripheral tolerance mechanisms. *Int. Immunol.* 32: 117–131.
22. Mouri, Y., M. Yano, M. Shinzawa, Y. Shimo, F. Hirota, Y. Nishikawa, T. Nii, H. Kiyonari, T. Abe, H. Uehara, et al. 2011. Lymphotoxin signal promotes thymic organogenesis by eliciting RANK expression in the embryonic thymic stroma. *J. Immunol.* 186: 5047–5057.
23. Morimoto, J., M. Matsumoto, R. Miyazawa, H. Yoshida, K. Tsuneyama, and M. Matsumoto. 2022. Aire suppresses CTLA-4 expression from the thymic stroma to control autoimmunity. *Cell Rep.* 38: 110384.
24. Mouri, Y., Y. Ueda, T. Yamano, M. Matsumoto, K. Tsuneyama, T. Kinashi, and M. Matsumoto. 2017. Mode of tolerance induction and requirement for Aire are governed by the cell types that express self-antigen and those that present antigen. *J. Immunol.* 199: 3959–3971.
25. Gillum, A. M., E. Y. Tsay, and D. R. Kirsch. 1984. Isolation of the *Candida albicans* gene for orotidine-5′-phosphate decarboxylase by complementation of *S. cerevisiae ura3* and *E. coli pyrF* mutations. *Mol. Gen. Genet.* 198: 179–182.
26. Tasaki, S., T. Cho, J. I. Nagao, S. Ikezaki, Y. Narita, K. I. Arita-Morioka, K. Yasumatsu, K. Toyoda, H. Kojima, and Y. Tanaka. 2018. Th17 cells differentiated with mycelial membranes of *Candida albicans* prevent oral candidiasis. *FEMS Yeast Res.* 18: foy018.
27. Hayashi, T., H. Ozaki, Y. Sasagawa, M. Umeda, H. Danno, and I. Nikaido. 2018. Single-cell full-length total RNA sequencing uncovers dynamics of recursive splicing and enhancer RNAs. *Nat. Commun.* 9: 619.
28. Picelli, S., A. K. Björklund, B. Reinius, S. Sagasser, G. Winberg, and R. Sandberg. 2014. Tn5 transposase and tagmentation procedures for massively scaled sequencing projects. *Genome Res.* 24: 2033–2040.
29. Hennig, B. P., L. Velten, I. Racke, C. S. Tu, M. Thoms, V. Rybin, H. Besir, K. Remans, and L. M. Steinmetz. 2018. Large-scale low-cost NGS library preparation using a robust Tn5 purification and tagmentation protocol. *G3 (Bethesda)* 8: 79–89.
30. Chen, S., Y. Zhou, Y. Chen, and J. Gu. 2018. fastp: an ultra-fast all-in-one FASTQ preprocessor. *Bioinformatics* 34: i884–i890.
31. Dobin, A., C. A. Davis, F. Schlesinger, J. Drenkow, C. Zaleski, S. Jha, P. Batut, M. Chaisson, and T. R. Gingeras. 2013. STAR: ultrafast universal RNA-seq aligner. *Bioinformatics* 29: 15–21.
32. Li, H., B. Handsaker, A. Wysoker, T. Fennell, J. Ruan, N. Homer, G. Marth, G. Abecasis, and R. Durbin; 1000 Genome Project Data Processing Subgroup. 2009. The sequence alignment/map format and SAMtools. *Bioinformatics* 25: 2078–2079.
33. Anders, S., P. T. Pyl, and W. Huber. 2015. HTSeq—a Python framework to work with high-throughput sequencing data. *Bioinformatics* 31: 166–169.
34. Robinson, M. D., D. J. McCarthy, and G. K. Smyth. 2010. edgeR: a Bioconductor package for differential expression analysis of digital gene expression data. *Bioinformatics* 26: 139–140.
35. Gu, Z., R. Eils, and M. Schlesner. 2016. Complex heatmaps reveal patterns and correlations in multidimensional genomic data. *Bioinformatics* 32: 2847–2849.
36. Yu, G., L. G. Wang, Y. Han, and Q. Y. He. 2012. clusterProfiler: an R package for comparing biological themes among gene clusters. *OMICS* 16: 284–287.
37. Lindmark, E., Y. Chen, A. M. Georgoudaki, D. Dudziak, E. Lindh, W. C. Adams, K. Loré, O. Winqvist, B. J. Chambers, and M. C. Karlsson. 2013. AIRE expressing marginal zone dendritic cells balances adaptive immunity and T-follicular helper cell recruitment. *J. Autoimmun.* 42: 62–70.
38. Guilliams, M., C. A. Dutertre, C. L. Scott, N. McGovern, D. Sichien, S. Chakarov, S. Van Gassen, J. Chen, M. Poidinger, S. De Prijck, et al. 2016. Unsupervised high-dimensional analysis aligns dendritic cells across tissues and species. *Immunity* 45: 669–684.
39. Ohl, L., M. Mohaupt, N. Czeloth, G. Hintzen, Z. Kiafard, J. Zwirner, T. Blankenstein, G. Henning, and R. Förster. 2004. CCR7 governs skin dendritic cell migration under inflammatory and steady-state conditions. *Immunity* 21: 279–288.

40. Randolph, G. J., V. Angeli, and M. A. Swartz. 2005. Dendritic-cell trafficking to lymph nodes through lymphatic vessels. *Nat. Rev. Immunol.* 5: 617–628.
41. Fergusson, J. R., M. D. Morgan, M. Bruchard, L. Huitema, B. A. Heesters, V. van Unen, J. P. van Hamburg, N. N. van der Wel, D. Picavet, F. Koning, et al. 2019. Maturing human CD127+ CCR7+ PDL1+ dendritic cells express AIRE in the absence of tissue restricted antigens. *Front. Immunol.* 9: 2902.
42. Hemmi, H., K. Hoshino, and T. Kaisho. 2016. In vivo ablation of a dendritic cell subset expressing the chemokine receptor XCR1. *Methods Mol. Biol.* 1423: 247–253.
43. Kisand, K., A. S. Bøe Wolff, K. T. Podkrajsek, L. Tserel, M. Link, K. V. Kisand, E. Ersvaer, J. Perheentupa, M. M. Erichsen, N. Bratanic, et al. 2010. Chronic mucocutaneous candidiasis in APECED or thymoma patients correlates with autoimmunity to Th17-associated cytokines. *J. Exp. Med.* 207: 299–308.
44. Puel, A., R. Döffinger, A. Natividad, M. Chrabieh, G. Barcenas-Morales, C. Picard, A. Cobat, M. Ouachée-Chardin, A. Toulon, J. Bustamante, et al. 2010. Autoantibodies against IL-17A, IL-17F, and IL-22 in patients with chronic mucocutaneous candidiasis and autoimmune polyendocrine syndrome type I. *J. Exp. Med.* 207: 291–297.
45. Gardner, J. M., T. C. Metzger, E. J. McMahon, B. B. Au-Yeung, A. K. Krawisz, W. Lu, J. D. Price, K. P. Johannes, A. T. Satpathy, K. M. Murphy, et al. 2013. Extrathymic Aire-expressing cells are a distinct bone marrow-derived population that induce functional inactivation of $CD4^+$ T cells. *Immunity* 39: 560–572.
46. Delong, T., T. A. Wiles, R. L. Baker, B. Bradley, G. Barbour, R. Reisdorph, M. Armstrong, R. L. Powell, N. Reisdorph, N. Kumar, et al. 2016. Pathogenic CD4 T cells in type 1 diabetes recognize epitopes formed by peptide fusion. *Science* 351: 711–714.
47. Gillis-Buck, E., H. Miller, M. Sirota, S. J. Sanders, V. Ntranos, M. S. Anderson, J. M. Gardner, and T. C. MacKenzie. 2021. Extrathymic *Aire*-expressing cells support maternal-fetal tolerance. *Sci. Immunol.* 6: eabf1968.
48. Nishijima, H., M. Matsumoto, J. Morimoto, K. Hosomichi, N. Akiyama, T. Akiyama, T. Oya, K. Tsuneyama, H. Yoshida, and M. Matsumoto. 2022. Aire controls heterogeneity of medullary thymic epithelial cells for the expression of self-antigens. *J. Immunol.* 208: 303–320.